Doctoral dissertation

Study on Degradation Analyses of Electrolyte Membranes for Proton Exchange Membrane Fuel Cells with NMR

December, 2013

Mari Takasaki

Study on Degradation Analyses of Electrolyte Membranes for Proton Exchange Membrane Fuel Cells with NMR

Chapter 1 Introduction to this study

Chapter 2 Structural Analysis of a Perfluorosulfonate Ionomer in Solution by ^{19}F and ^{13}C NMR

Chapter 5 Conclusions of this study

Chapter 1 Introduction

1.1. Introduction to Chapter 1

Nowadays, human beings significantly depend on petroleum resources as energy sources, especially fossil fuels. However, petroleum resources will be exhausted near future, the development of new resources such as shale gas, methane hydrate, or biofuel by an enzyme reaction has increased recently. When converting fossil fuels such as petroleum, shale gas, methane hydrate and so on into energy, carbon dioxide, i.e., greenhouse-effect gases are emitted. With the generation of such greenhouse-effect gases, the global environment has become rapidly abnormal. To prevent aggravation, drastic reductions of greenhouse-effect gas emissions are urgently required. To this end, energy sources that have a low environmental impact, generate less amounts of greenhouse-effect gases, and can be replaced by petroleum resources are needed.

In recent years, hydrogen as a new energy source and a fuel cell that uses hydrogen have attracted significant attention. Although the power generation efficiency of a fuel cell is high, it is possible to acquire a higher efficiency by introducing a cogeneration system. In a cogeneration system, secondary energy, such as thermal energy which arises with reactions, is utilized by a hot-water supply system. Since fuel cells do not emit environmental pollutants, such as carbon dioxide, NO_x, and SO_x, they are desirable in terms of environmental pollution prevention. A fuel cell is classified according to the quality of the material of an electrolyte layer or operating temperature. In particular, a proton-exchange membrane fuel cell (PEMFC) operates from room temperature to about 100°C in a comparatively low-temperature region. Compared with other fuel cells that operate at high temperature, it is excellent with respect to its function of operating temperature or miniaturization. Therefore, wide applicability is expected, e.g., as power supply for electric vehicles and portable electronic devices and for home use (for stationing). As a result, automobile and electrical equipment manufacturers all over the world are focusing on development.

1.2. Power generation principle and the composition of PEMFCs

1.2.1. Power generation principle

Typically, an electrolyte layer in PEMFCs is an ion-exchange membrane made from a macromolecule. A fuel electrode and an air electrode are incorporated into each side of

the membrane. When a reactive gas is supplied to both electrodes, an electrode reaction occurs at the "three-phase interface," where an electrode catalyst, an electrolyte, and the reactive gas are adjacent to each other.[1] The reaction in expression (1) occurs at the fuel electrode; i.e., hydrogen is oxidized, and a proton (H+) and electrons are generated. This proton moves to the air electrode while attached to a water molecule. An electron passes along an external circuit at this time.

$H_2 \rightarrow 2H+ \ +2e-$ (1)

Expression (2) shows the reaction at the air electrode. As shown in expression (2), the protons and electrons that moved from the fuel electrode are used to reduce oxygen, which results in the generation of water:

$1/2O_2 + 2H+ + 2e- \rightarrow H_2O$ (2)

Expression (3) shows the equation of complete reaction occurring in a PEMFC. In the electrode reaction of a PEMFC, no carbon dioxide is emitted, as shown in expression (3):

$H_2 + 1/2O_2 \rightarrow H_2O$ (3)

1.2.2. Composition of a PEMFC single cell

A polyelectrolyte membrane serves as a proton conductor in a PEMFC. Both sides of the polymer electrolyte membrane are coated with catalyst layers composed of carbon-supported platinum. Carbon-supported platinum is produced via the distribution of platinum particles (3 to 5 nm in diameter) onto carbon particles (20 to 30 nm in diameter). A gas diffusion layer (GDL), which promptly supplies reactive gas to the catalyst layer, is arranged on the catalyst layer surface. The porous object constructed from carbon fiber paper or cloth is used for the GDL. The assembly in which the catalyst layer and the GDL are joined to the polyelectrolyte membrane is referred to as the membrane electrode assembly (MEA). A separator used to channel the reactive gas and electron collecting boards is arranged on both sides of the MEA and comprises a unit cell (i.e., a single cell). In a PEMFC system, single cells are typically laminated into tens or hundreds of cells connected in series to form a stacked cell.

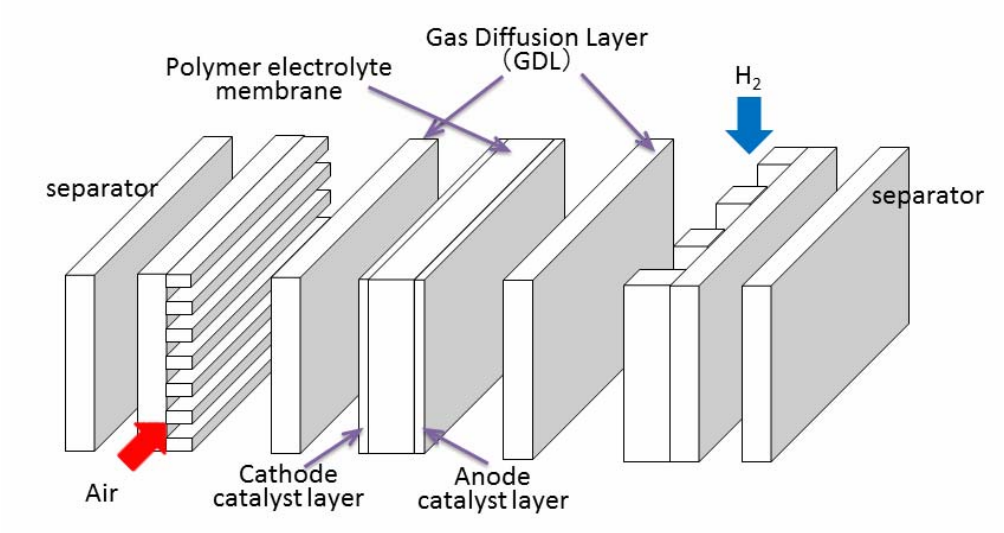

Figure 1-1. Composition of a PEMFC single cell

1.3. Constructional elements of PEMFCs and research tasks

Although PEMFCs are expected to be leading candidates for next-generation power supplies, numerous issues need to be overcome before they can be utilized. Cost reduction is an especially pressing need. According to the road map of the New Energy and Industrial Technology Development Organization (NEDO), an independent administrative agency, the delivery price for stationing PEMFCs was 2 million yen at the time of their introduction in 2009. The cost targets for stationing are as follows: 1) by approximately 2015 (spread term), 500,000 to 700,000 yen; 2) by approximately 2020 (spread expansion term), 400,000 yen; and, 3) by approximately 2030 (full-scale spread term), 400,000 yen or less. On the other hand, the cost of a fuel-cell electric vehicle was tens of millions of yen in 2010, and the price target for an electric vehicle is as follows: 1) by approximately 2015 (present-condition technology), 1 million yen; and, 2) by approximately 2025 (full-scale commercialization term), 500,000 yen or less.[2] Achieving such cost targets by solely relying on the mass production effect is difficult, and extensive improvements in the durability and performance of PEMFCs, including the elucidation of the reaction or degradation mechanisms, are indispensable toward achieving these targets. The research and development of PEMFCs is under active development in every industrialized country in the world. Below, the constructional elements of PEMFCs and the research tasks toward their extensive utilization are described.

1.3.1. Research tasks of polyelectrolyte membranes

Polymer electrolytes are used as electrolyte membranes and as electrodes in PEMFCs. The following characteristics are required of polyelectrolyte membranes intended for use in PEMFCs: high ionic conductivity, impermeability to reactive gases, good chemical and mechanical strength, and good electrically insulating properties. Furthermore, for electric vehicle applications, the abilities to rapidly start in a cold environment (approximately −30 °C) and to maintain high ionic conductivity under high-temperature and low-humidity conditions are important. Two types of electrolyte membranes have been developed for PEMFCs: perfluorosulfonic acid (PFSA) membranes and hydrocarbon membranes.

1.3.1.1. PFSA electrolyte membranes

Nafion® by DuPont, Flemion® by Asahi Glass, Aciplex® by Asahi Chemicals, and Dow® by Dow Chemical are commercial PFSA electrolyte membranes that are currently available. The chemical structure of the polymer that constitutes each membrane is shown in Figure 1-2. Nafion®, the first polymer with high ionic conductivity, was discovered by Walther Grot of E. I. du Pont de Nemours & Co. in the 1960s.[3] The high ionic conductivity of Nafion® results from the incorporation of tetrafluoroethylene into a perfluoro vinyl ether with a sulfo group.[4, 5] Neither negative ions nor electrons migrate through Nafion® membranes; only positive ions are transported through them. With respect to the structure of the membrane that generates the high ion-conductivity of PFSA electrolyte membranes, the opinion advocated by Gierke and others is known widely: the sulfo groups in the side chains of the PFSA polymer, along with water molecules, compose a cluster with a diameter of approximately 10 Å, and positive ions move inside of these clusters.[6] Moreover, the cluster structure of the PFSA electrolyte membrane has been proven by X-ray diffraction (XRD) and small-angle X-ray scattering (SAXS) analyses.[7, 8, 9] Therefore, the high ionic conductivity of a PFSA electrolyte membrane is determined by the following three conditions: 1) the number of sulfo groups per unit area, 2) the water content in the electrolyte membrane, and 3) the size of the ionic channel.

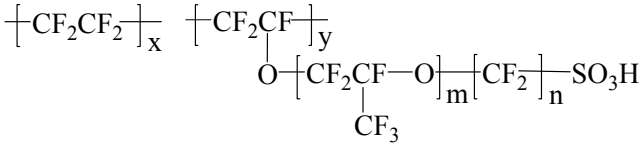

Figure 1-2. Chemical structure of the PFSA polymer electrolyte

1.3.1.2. Hydrocarbon electrolyte membranes

Because a dramatic cost reduction in PEMFCs can be realized by the use of a hydrocarbon electrolyte membrane, the development of such membranes have been enthusiastically promoted as replacements for PFSA electrolyte membranes. Polymers for current hydrocarbon electrolyte membranes include sulfonated poly(arylene ether sulfone)s,[10, 11] poly(arylene ether ether ketone)s (SPEEK),[12, 13, 14] poly(arylene sulfide sulfone)s,[15, 16] polyimides,[17, 18, 19] poly(arylene ether nitrile)s,[20] polybenzimidazoles,[21, 22] and polyphenylenes,[23, 24] among others. The chemical stability and durability of such membranes have been inferior to those of PFSA electrolyte membranes, and the realization of initial characterization equivalent to that has been also difficult. The initial characterization of some recently developed hydrocarbon electrolyte membranes has shown them to be equivalent to PFSA electrolyte membranes. Going forward, the creation of hydrocarbon membranes with better durability and better chemical stability based on their degradation mechanisms will be an active area of research.

1.3.1.3. Research tasks of electrolyte membranes

The goal of this study on electrolyte membranes is to create sufficiently durable membranes that exhibit high ionic conductivity under high-temperature and low-humidity conditions. Membranes intended for use in PEMFCs in electric vehicles should exhibit 1) heat resistance to temperatures of approximately 120°C, 2) sufficient ion conductivity under low-humidity conditions, and 3) sufficient mechanical strength. With respect to the durability of electrolyte membranes, Asahi Glass and Asahi Chemical have reported that they improved the mechanical strength of PFSA electrolyte membranes at high temperatures by controlling their molecular structures.[25, 26] With respect to membrane reinforcement, some trials of membranes with improved physical properties, such as improved mechanical strength, have also been reported.[27-30] Research on the use of electrolyte membrane degradation mechanisms to provide feedback for electrolyte membrane design is discussed later.

PFSA membranes also suffer shortcomings, such as high production cost and lack of environmental adaptability.[31-33] The production cost, in particular, is one of the factors that increases the cost of a PEMFC. Consequently, the development of outstanding PFSA electrolytes and inexpensive hydrocarbon electrolyte membranes that do not incorporate fluoride has been active research areas.

1.3.1.4. Degradation of electrolyte membranes

The failure of a fuel cell has been shown to originate by the interaction of numerous

degradation mechanisms of the components comprising a fuel cell. Therefore, we discuss the degradation mechanisms of each component as well as that of a membrane. The currently argued degradation phenomena for components other than the membrane include the dissolution of catalytic platinum particles,[34-36] the corrosion of the carbon-supported catalyst,[37-40] the delamination of the electrode and membrane layers,[41, 42] the reduction of the electrochemically active surface area of the catalyst, and an increase in the size of Pt particles.[43] However, a major reason for the failure of fuel cells is the degradation of the polymer electrolyte membrane. The degradation mechanisms of membranes are investigated and the improvement in durability of membranes is attained through feedback from a given membrane design. Hence, detailed investigations of membranes' degradation mechanisms contribute to performance gains in PEMFCs and have important implications with respect to their widespread adaptation.

Numerous investigations into PFSA electrolyte membrane degradation have been reported, and various phenomena have been revealed by a wide array of analysis techniques, including

1) the detection of fluoride ion released into wastewater; [44-51]
2) membrane thinning;[52]
3) pinhole and/or crack formation;[50, 51, 53-57]
4) chemical degradation (which is considered the most important mode of PEMFC failure);[42, 44, 45, 52, 58]
5) decreased ion-exchange capacity;[57]
6) changes in pH;[45]
7) decreased conductivity;[45, 59]
8) reduced membrane thickness;[52]

The analysis techniques used to investigate degradation phenomena, including

1) broadband dielectric spectroscopy;[60]
2) electron paramagnetic resonance (EPR);[41, 42, 58, 61-68]
3) Fourier-transform infrared spectroscopy (FT-IR);[44, 49, 53, 56, 61, 69-72]
4) Raman spectroscopy;[61]
5) UV–visible spectroscopy;[61]
6) liquid NMR;[53, 73, 74]
7) solid-state NMR;[49. 53, 70, 75]
8) mass spectroscopy;[73, 74]
9) X-ray photoelectron spectroscopy (XPS);[43, 55, 69, 76, 77]

10) wide-angle and small-angle X-ray diffraction;[43, 55]

11) thermogravimetric analysis (TGA);[56, 57, 78]

12) transmission electron microscopy (TEM)[79] and scanning electron microscopy (SEM).[53]

Membrane degradation mechanisms that should be investigated include the following. During the operation of a fuel cell, the membrane is exposed to a chemically oxidizing environment on the cathode side and is exposed to a chemically reducing environment on the anode side. Moreover, gas crossover is directly related to radical formation. Actually, the main cause of the chemical degradation of electrolyte membranes is considered to be attack by radicals. The degradation of electrolyte membranes has been experimentally shown to be based on HO• and HOO• radical formation in studies in which in situ fuel cell experiments were performed.[58] These radicals are generated from both electrochemical and chemical reactions and form at both the anode and the cathode sides. Also, the CF carbon in the main chain of Nafion® has been reported to be a radical center.[42, 65] After the UV irradiation of Nafion® membranes in a hydroperoxide solution containing metal ions, chain-end radicals with structures such as -O-CF_2-CF_2• were identified by EPR.[65] The exposure of PFSA membranes to the Fenton's test resulted in diminished fluoride and sulfur signals in the XPS spectrum. This result was in agreement with the quantities of fluoride and sulfuric acid ions released.[69] Similarly, FT-IR spectroscopy has been used to demonstrate the bridge formation of C=O and S–O–S units in degraded membranes, and the latter units indicate the presence of sulfonic acid groups in the side chains.[70, 71] ^{19}F NMR and MS analyses of degraded Nafion® in solution showed the existence of low-molecular-weight compounds, which were fragments of the Nafion® side-chain structure.[73] However, various reaction processes involved in the chemical degradation of the membrane, details of the structural changes in the degraded membrane, and the quantities of the decomposition products were not elucidated, and they remain subjects of investigation.

The degradation of hydrocarbon membranes has also been investigated.[80, 81] Since different membrane materials have been proposed, research on these membranes is not as advanced as that on PFSA membranes. Typically, the amount of fluoride ion released into wastewater is used as an index of the extent of degradation of a PFSA membrane. However, in the case of hydrocarbon membranes, this index is not useful. Thus, we discuss studies based on approaches that differ from those used for PFSA membranes.

1.3.1.5. Degradation of electrolyte membranes by NMR

This study was aimed at investigating the degradation mechanisms of electrolyte membranes by NMR. Therefore, the features of NMR that are useful for this purpose and the reasons for having adopted this technique are explained here.

As previously mentioned, various techniques are used to investigate the degradation mechanisms of fuel cells. Therefore, the techniques used need to be selected and combined according to the phenomenon being investigated and the features and type of the sample under investigation. Techniques for investigating the general chemical structure of a sample include NMR, MS, IR, X-ray diffraction, among others. Among these techniques, NMR is the most useful technique to study the degradation analysis of electrolyte membranes. The features of NMR that make it suitable for this purpose are listed below.

1) NMR can offer substantial and more information about the chemical structure, including the chemical shift, signal integration values, and signal divisions according to spin coupling between various nuclei (^{1}H, ^{13}C, ^{19}F, and so on).
2) The amount of the information related to chemical structures explosively increases with the use of various two-dimensional NMR techniques, and determinations of the chemical structures of samples with unknown chemical structures are possible.
3) The use of NMR enables the elucidation of the chemical structures of minor components of samples.
4) With NMR, all of the molecular species that exist in a sample are observed. Fundamentally, NMR signal intensity is proportional to the abundance ratio of the nuclei detected. However, in MS, ionic strength differs depending on the ionization efficiency. In FTIR, sensitivity differs for each absorption band.
5) With NMR, the target ingredient can be quantified by using reagents generally marketed as standard samples. In contrast, with MS and FT-IR, sensitivity corrections are required, and these corrections require that the target ingredients be used as standard substances.

For reasons of 1), 2), and 3), the chemical structures of pristine membranes, the membranes after operation, and degradation products with unknown chemical structures can be determined by NMR. The determination of the chemical structures and quantitative analysis of degradation products, which may be present in low concentrations and be inseparable, are also possible. In particular, the compounds generated by the degradation of polymers are typically present in low concentrations and cannot, in many cases, be isolated. Furthermore, for reasons of 4) and 5), a

quantitative analysis of compounds with special structures by NMR is possible by using chemical reagents as general standards. In contrast, MS and FTR cannot provide as much information related to the chemical structure as NMR. Moreover, with MS and FT-IR, the quantitative analysis of degradation products is not possible when the degradation products have special structures and are not commercially available. Although X-ray diffraction is also a useful structural determination technique, it is not suited for general-purpose use, because X-ray diffraction requires a single crystal of the target ingredient, and the preparation of such single crystals is difficult. Hence, NMR is indispensable for the study of the degradation of electrolyte membranes. However, as previously mentioned, the literature contains few reports of the analysis of degraded electrolyte membranes by NMR.

1.3.2. Research tasks of electrode catalysts

Platinum is accepted as an effective catalyst in PEMFCs. Although platinum is a highly active metallic element, it is very expensive because it is a precious metal. The use of platinum as a catalyst dramatically increases the cost of a PEMFC. Therefore, to reduce the cost of the electrode catalysts [82], many researchers have focused on reducing the amount of platinum[83-86] used and on developing non-platinum catalysts.[87, 88]

1.3.2.1. Alloy catalysts and compound catalysts

Alloy catalysts that provide high activation and stabilization of electrode catalysts are currently under development. Examples of alloy catalysts that effectively function as PEMFC catalysts have been reported. A typical anode alloy catalyst is PtRu/C. When only Pt is used as a catalyst with reformed gas for PEMFCs, platinum is poisoned by carbon monoxide mixed into the fuel gas, and the catalyst activity consequently decreases. The use of a PtRu/C catalyst diminishes the influence of this poisoning.[89-92] An investigation of this mechanism is in progress.[93] PtCo/C is a typical cathode catalyst.[94-98] Many studies of other alloy catalysts are also in progress.[99-101] However, the mechanism by which alloy catalysts function is unclear. The elucidation of the mechanism by which such catalysts function is important for the development of a highly active electrode catalyst.

Compound catalysts, such as oxides, nitrides, or metal complexes, have been studied as highly active catalysts to replace platinum.[87, 102, 103] Because precious metals are not used in compound catalysts, a substantial cost reduction can be reasonably expected. Some transition-metal compounds can be used as substitutes for platinum catalysts.[87] The utilization of compound catalysts requires further examination.

1.3.2.2. Reduction of the amount of catalyst used

The catalyst in a PEMFC functions only at the three-phase interface, where the electrolyte, catalyst, and reactive gas contact each other.[104] The supply of the reactive gas to the three-phase interface is significantly influenced by the porosity of a catalyst layer. Therefore, the control of the catalyst layer structure during MEA manufacturing processes becomes very important for the effective practical use of a catalyst.[105, 106]

The method of manufacturing a catalyst layer is as follows. First, catalyst powder is mixed using several types of solvents and electrolyte solutions, and the resulting catalyst ink is produced. Then, this catalyst ink is applied to an electrode surface. The electrodes are then placed on both sides of an electrolyte membrane, and they are joined.[105] Alternatively, after the catalyst ink has been applied to a resin board, it can be subsequently transferred to the electrolyte membrane.[106-109]

For this manufacturing process, an examination of numerous parameters, such as the temperature at the time of pressing, has been reported.[110] Furthermore, a platinum catalyst is effectively utilized by the optimization of the three-phase interface formed by an electrode catalyst and an electrolyte. Numerous investigations of methods to reduce the amount of platinum used based on the more effective utilization of platinum through the optimization of the three-phase interface have been reported. A reduction of the amount of platinum catalyst used and the characteristics of a power generation process as a function of time were reported in a study in which the structure of the three-phase interface was controlled.[83, 84] Although further reductions in the amount of platinum used in electric vehicle applications is necessary, research efforts in this area are producing steady progress.

1.3.2.3. Catalyst support

Platinum, which is expensive, is commonly used as the electrode catalyst in PEMFCs. Hence, the efficient use of the electrode catalyst is required. Platinum particles with sizes on the order of several nanometers and that are fixed onto particles several tens of nanometer in size are now used as catalysts. The particles used as the support medium of these platinum particles are referred to as the "support." Carbon black is generally used as the support.[111] The biggest drawback to this approach is the corrosion of the support.[112] In particular, carbon on the cathode side of a PEMFC corrodes under high potential and in the presence of hydrogen peroxide generated by a sub-reaction. The support is degraded, which leads to catalyst degradation through the loss and aggregation of catalyst particles. The most effective approach to this problem is to

increase the crystallinity of carbon black to inhibit the corrosion of the support. However, increasing the crystallinity of carbon black also inhibits the dispersibility of platinum particles and accelerates the aggregation of platinum particles.

Research on the use of carbon nanotubes with a comparatively high degree of crystallinity as a catalyst support is also in progress.[113-116] Moreover, unlike carbon black, carbon nanotubes are fibrous. Therefore, they can be easily formed into three-dimensional vesicular structures when the catalyst layer is formed; their fibrous nature also improves the permeability of a gas to the catalyst layer. As a result, the effective use of catalysts has been identified as an urgent need,[116-118] and studies on this topic continue.

1.4. Purpose and composition of this paper

1.4.1. Purpose of this paper

As previously mentioned, the research tasks related to each constructional element need to be solved to realize the large-scale utilization of PEMFCs, and especially to realize large-scale utilization in electric vehicles. In particular, improvements in the durability and performance of polyelectrolyte membranes are indispensable. In research on improvements in the durability of polyelectrolyte membranes, information related to the degradation of a membrane is used as feedback on a given membrane design, which in turn, leads to the creation of new membranes. To investigate the degradation of a membrane, the determination of the chemical structure of a pristine membrane, as well as that of a degraded membrane, is necessary. In addition, it is necessary to improve the functions of the membranes. Moreover, all assignments of NMR signals of pristine membranes are also indispensable in the NMR structural analysis of the degradation products.

This study aimed to determine the chemical structures of two pristine membrane materials (i.e., PFSA and the hydrocarbon electrolyte SABC (sulfonated aromatic block copolymer)) and the assignments of all of their NMR signals. In addition, it aimed to elucidate the degradation mechanisms by investigating the chemical structures and the quantity of the degradation products from PFSA electrolytes obtained after PEMFC operation tests and an accelerated degradation tests.

1.4.2. Composition of this paper

The text in this study consists of three chapters: Chapter 2 to Chapter 4.

In Chapter 2, the structural analysis of Nafion® (the representative PFSA polymer) by two-dimensional NMR and the assignments of all of the NMR signals (^{19}F and ^{13}C) of Nafion® are described. For Nafion® in solution, exact assignments of the chemical shifts in the ^{19}F NMR and ^{13}C NMR spectra have not been previously reported. Although Nafion® is sold as a solution, it is actually a dispersion. Therefore, in the two-dimensional NMR spectra of the solution state, marginal information of the chemical structure was obtained. Consequently, two model compounds (PFTTF and PFSA), whose chemical structures partially correspond with that of Nafion® were used. The model compounds were structurally analyzed by two-dimensional NMR methods, and all of the ^{19}F and ^{13}C NMR signals of Nafion® were assigned. The studies contain few reports of the two-dimensional NMR structural analysis of fluorine compounds. In this study, a two-dimensional NMR analytical method for a fluorine compound consisting of a combination of ^{19}F–^{19}F COSY, ^{19}F–^{13}C HSQC, and ^{19}F–^{13}C HMBC is proposed. Part of the structural analysis strategy for the fluorine compound proposed here demonstrates the usefulness of the structural determination of the decomposition products of the PFSA polymer quantified in Chapter 3. However, Chapter 3 provides assignments of only the ^{19}F NMR signals and does not include the structural analysis. The assignments of the ^{19}F NMR signals of Nafion® obtained here serve as basic data in our investigation of PFSA polymer degradation products.

In Chapter 2, the PFSA polymer electrolyte is referred to as “perfluorosulfonate ionomer.”

In Chapter 3, the degradation of the PFSA polymer in two tests was primarily investigated by NMR.

One test was PEMFC operation tests in OCV-hold and load-cycling modes. The degradation products of the PFSA polymer after the operation tests were divided into low-molecular-weight and high-molecular-weight components, and they were subsequently investigated. For the low-molecular-weight degradation products, quantitative analysis based on the structures acquired from the NMR structural analysis method described in Chapter 2 and their NMR signal assignments was performed. The quantities of the low-molecular-weight degradation products have not been previously reported and are quantified for the first time in this paper. With respect to the high-molecular-weight degradation products, the degraded PFSA polymer was dissolved, and the structures of the side and main chains were subsequently investigated. In addition, the low-molecular-weight degradation products were primarily obtained from the catalyst layer. Reactions in PEMFCs are known to occur at the three-phase

interface. Hence, we expected that the PFSA polymer in the catalyst layer degraded. The degradation products of the PFSA polymer in the catalyst layers were therefore investigated in detail.

The second degradation test consisted of hydrogen peroxide vapor (HPV) exposure tests of PFSA polymer membranes. It is one of the accelerated degradation tests; it is considered that HPV is the main cause of membrane degradation. PFSA polymer degradation occurring during the tests was investigated by ion chromatography and total organic carbon analysis of trap water and by ^{19}F NMR to analyze the water/methanol extracts from the membranes. The amounts of total organic carbon, fluoride ion, TFA(s), and decomposition products in the membranes were compared with the membrane weight loss due to degradation, and the degradation was systematically elucidated.

In Chapter 2, the PFSA polymer electrolyte was indicated as being a PFSA polymer, because the membranes and the PFSA polymer electrolyte in a catalyst layer were evaluated.

As previously discussed, reductions in the costs of PEMFCs are necessary to enable their broad utilization. In Chapter 4, the NMR structural analysis of a hydrocarbon polymer electrolyte is described; such membranes play an important role in reducing the cost of PEMFC membranes. SABC, which consists of hydrophobic and hydrophilic blocks, exhibits physical properties almost equivalent to those of PSFA membranes. SABC was analyzed by various two-dimensional NMR methods. Because of its complicated chemical structure that includes five different phenylene rings, ^{1}H and ^{13}C signals were observed in a narrow chemical-shift range. By improving the separation of the NMR signals, we attained perfect assignments of the ^{1}H and ^{13}C NMR signals for SABC. The ion-exchange capacity and the copolymerization composition were calculated from the ^{1}H NMR assignments for SABC. In this study, all of the assignments of the ^{13}C NMR signals of SABC were attained for the first time, and the chemical structure was determined. The analysis method for SABC and the assignments of ^{1}H and ^{13}C NMR signals obtained here serve as foundation data for the investigation of SABC degradation products.

1.5. Reference of chapter 1

1. T. Hirai, T. Kinumoto, K. Kikuchi, K. Uzawa, Y. Uchimoto, Y. Uchimoto, Z. Ogumi, *47th Battery Symposium in Japan preprints* **2006**.
2. NEDO, Fuel cell and a hydrogen technology development road map 2010

3. C. Steven, *The News Journal* **2006**, B7.
4. C. Heitner-Wirguin , *J. Membr. Sci.*, **1996**, *120*, 1.
5. K. A. Mauritz , R. B. Moore, *Chem. Rev. (Washington, DC, U. S.)* **2004**, *104*, 4535
6. T. D. Gierke, G. E. Munn, F. C. J. Wilson, *J. Polym. Sci.,Part B: Polym. Phys.*, **1981**, *19*, 1687
7. J. A. Elliott, S. Hanna, A. M. S. Elliott, G. E. Cooley, *Macromolecules* **2000**, *33*, 4161.
8. E. J. Roche, M. Pineri, R. Duplessix, A. M. Levelut, *J. Polym. Sci, Polym. Phys. Ed*. **1981**, *19*, 1.
9. J. A. Elliotta, S. Hannaa, A. M. S. Elliottb, G. E. Cooleyc, *Polymer* **2001**, *42*, 2251.
10. F.Wang, M.Hickner, Y. S. Kim, T. A. Zawodzinski, J. E. McGrath, *J. Membr. Sci.* **2002**, *197*, 231.
11. Y. Chikashige, Y. Chikyu, K.Miyatake, M.Watanabe, *Macromolecules* **2005**, *38*, 7121.
12. P. Xing, G. P. Robertson, M. D. Guiver, S. D. Mikhailenko, K. Wang, S. Kaliaguine, *J. Membr. Sci*. **2004**, *229*, 95.
13. M. Gil, X. Ji, X. Li, H. Na, J. E. Hampsey, Y. Lu, *J. Membr. Sci.* **2004**, *234*, 75.
14. X. Shang, S. Tian, L. Kong, Y. Meng, *J. Membr. Sci.* **2005**, *266*, 94.
15. M. Schuster, K.-D. Kreuer, H. T. Andersen, J. Maier, *Macromolecules* **2007**, *40*, 598.
16. Z. Bai, T. D**.** Dang, *Macromol. Rapid Commun*. **2006**, *27*, 1271**.**
17. K. Miyatake, H. Zhou, T. Matsuo, H. Uchida, M. Watanabe, *Macromolecules* **2004**, *37*, 4961.
18. Y. Yin, Y.Suto, T. Sakabe, S. Chen, S. Hayashi, T.Mishima, O. Yamada, K.Tanaka, H. Kita, K.-i. Okamoto, *Macromolecules* **2006**, *39*, 1189.
19. J. Saito, K. Miyatake, M. Watanabe, *Macromolecules* **2008**, *41*, 2415.
20. Y. Gao, G. P. Robertson, D.-S. Kim, M. D. Guiver, S. D. Mikhailenko, X. Li, S. Kaliaguine, *Macromolecules* **2007**, *40*, 1512.
21. J. S. Wainright, J.-T. Wang, D. Weng, R. F. Savinell, M. Litt, *J. Electrochem. Soc.* **1995**, *142*, L121.
22. X. Glipa, M. El Haddad, D. J. Jones, J. Rozi_ere, *Solid State Ionics* **1997**, *97*, 323.
23. T. Kobayashi, M. Rikukawa, K.Sanui, N. Ogata, *Solid State Ionics* **1998**, *106*, 219.
24. C. H. Fujimoto, M. A. Hickner, C. J. Cornelius, D. A. Loy, *Macromolecules* **2005**, *38*, 5010.

25. M. Wakizoe, A. V. Omourtag, S. Srinivasan, *Electrochimica Acta* **1995**, *40*, 335.
26. N. Yoshida, T. Ishisaki, A. Watakabe, M. Yoshitake, *Electrochimic Acta* **1998**, *43*, 3749.
27. S. Hommura, Y. Kunisa, I. Terada, M. Yoshitake, *J. Fluorine Chem*. **2003**, *120*, 151.
28. B. Lakshmanan, W. Huang, D. Olmeijer, J. W. Weidner, *Electrochem. Solid-State Lett.* **2003**, *6*, A282.
29. H. Munakata, D. Yamamoto, K. Kanamura, *Journal of Power Sources* **2008**, *178*, 596.
30. A. Matsuda, N. Nakamoto, K. Tadanaga, T. Minami, M. Tatsumisago, *Solid State Ionics* **2003**, *247*, 162.
31. J. Rozi_ere, D. Jones, *J. Annu. Rev. Mater. Res.* **2003**, *33*, 503.
32. B. Lakshmanan, W. Huang, D. Olmeijer, J. W. Weidner, *Electrochem. Solid-State Lett.* **2003**, *6*, A282.
33. M. F. Mathias, R. Makharia, H.A.Gasteiger, J. J. Conley, T. J. Fuller, C. J.Gittleman, S. S. Kocha, D. P. Miller, C. K. Mittelsteadt, T. Xie, S. G. Yan, P. T. Yu, *Interface* **2005**, *14*, 24.
34. R. M. Darling, J. P. Meyers, *J. Electrochem. Soc.* **2005**, *152*, A242.
35. W. Bi, G. E. Gray, T. F. Fuller, *Electrochem. Solid-State Lett.* 2007, *10*, B101.
36. R. M. Darling, J. P. Meyers, *J. Electrochem. Soc.* **2003**, *150*, A1523.
37. J. P. Meyers, R. M. Darling, *J. Electrochem. Soc.* **2006**, *153*, A1432.
38. H. Tang, Z. G. Qi, M. Ramani, J. F. Elter, *J. Power Sources* **2006**, 158, 1306.
39. Z. Luo, D. Li, H. Tang, M. Pan, R. Ruan, *Int. J. Hydrogen Energy* **2006**, 31, 1831.
40. D. A. Stevens, M. T. Hicks, G. M. Haugen, J. R. Dahn, *J. Electrochem. Soc.* **2005**, *152*, A2309.
41. A. Bosnjakovic, S. Schlick, *J. Phys. Chem. B* **2006**, *110*, 10720.
42. A. Bosnjakovic, M. K. Kadirov, S. Schlick, *Res. Chem. Intermed.* **2007**, *33*, 677.
43. Z. B. Wang, P. J.Zuo, Y. Y. Chu, Y. Y. Shao, G. P. Yin, Int. *J. Hydrogen Energy* **2009**, *34*, 4387.
44. E. N. Balko, J. T. Chaklos, *J. Appl. Polym. Sci.* **1981**, *26*, 1519.
45. A. Pozio, R. F. Silva, M. De Francesco, L. Giorgi, *Electrochim Acta* **2003**, *48*, 1543.
46. M. Aoki, H. Uchida, M. Watanabe, *Electrochem. Commun.* **2005**, *7*, 1434.
47. V. O. Mittal, H. R. Kunz, J. M. Fenton, *Electrochem. Solid-State Lett.* **2006**, *9*, A299.

48. V. O. Mittal, H. R. Kunz, J. M. Fenton, *J. Electrochem. Soc.* **2006**, *153*, A1755.
49. T. Kinumoto, M. Inaba, Y.Nakayama, K. Ogata, R.Umebayashi, A.Tasaka, Y. Iriyama, T. Abe, Z. Ogumi, *J. Power Sources* **2006**, *158*, 1222.
50. W. Liu, K. Ruth, G. Rusch, *J. New Mater. Electrochem. Syst.* **2001**, *4*, 227.
51. M. Aoki, H. Uchida, M. Watanabe, *Electrochem. Commun.* **2006**, *8*, 1509.
52. V. O. Mittal, H. R. Kunz, J. M. Fenton, *J. Electrochem. Soc.* **2007**, *154*, B652.
53. H. L.Tang, P. K. Shen, S. P. Jiang, W. Fang, P. Mu, *J. Power Sources* **2007**, *170*, 85.
54. A. Collier, H. J. Wang, X. Z. Yuan, J. J. Zhang, D. P. Wilkinson, I*nt. J. Hydrogen Energy* **2006**, *31*, 1838.
55. C. D. Huang, K. S. Tan, H. Y. Lin, K. L. Tan, *Chem. Phys. Lett.* **2003**, *371*, 80.
56. M. L. Mittleman, J. R. Thomsen, C. A. Wilkie, *Chem. Abstr.* **1990**, *200*, 211.
57. J. Surowiec, R. Bogoczek, J. *Therm. Anal.* **1988**, *33*, 1097.
58. M. Danilczuk, F. D. Coms, S. Schlick, *J. Phys. Chem. B* **2009**, *113*, 8031.
59. M. Schulze, N. Wagner, T. Kaz, K. A. Friedrich, *Electrochim. Acta* **2007**, *52*, 2328.
60. D. W. Rhoades, M. K. Hassan, S. J. Osborn, R. B. Moore, K. A.Mauritz, *J. Power Sources* **2007**, *172*, 72.
61. S. H. Almeida, Y. Kawano, *Polym. Degrad. Stab.* **1998**, *62*, 291.
62. A. Panchenko, H. Dilger, J. Kerres, M. Hein, A. Ullrich, T.Kaz, E. Roduner, *Phys. Chem. Chem. Phys.* **2004**, *6*, 2891.
63. B. Vogel, E. Aleksandrova, S. Mitov, M. Krafft, A. Dreizler, J. Kerres, M. Hein, E. Roduner, *J. Electrochem. Soc.* **2008**, *155*, B570.
64. M. Danilczuk, A. Bosnjakovic, M. K. Kadirov, S. Schlick, *J. Power Sources* **2007**, *172*, 78.
65. M. K. Kadirov, A. Bosnjakovic, S. Schlick, *J. Phys. Chem. B* **2005**, *109*, 7664.
66. A. Panchenko, H. Dilger, E. Moller, T. Sixt, E. Roduner, *J. Power Sources* **2004**, *127*, 325.
67. A. Lund, L. D. Macomber, M. Danilczuk, J. E. Stevens, S. Schlick, **J.** *Phys. Chem. B* **2007**, *111*, 9484.
68. E. Endoh, *Electrochem. Solid-State Lett.* **2004**, *7*, A209.
69. C. Chen, G. Levitin, D. W. Hess, T. F. Fuller, *J. Power Sources* **2007**, *169*, 288.
70. F. M. Collette, C. Lorentz, G. Gebel, F. Thominette, *J. Membr. Sci.* **2009**, *330*, 21.
71. J. L. Qiao, M. Saito, K. Hayamizu, T. Okada, *J. Electrochem. Soc.* **2006**, *153*, A967.
72. T. Xie, C. A. Hayden, *Polymer* **2007**, *48*, 5497.

73. J. Healy, C. Hayden, T.Xie, K.Olson, R. Waldo, A. Brundage, H. Gasteiger, J. Abbott, *Fuel Cells* **2005**, *5*, 302.
74. C. Zhou, M. A. Guerra, Z. M.Qiu, T. A. Zawodzinski, D. A. Schiraldi, *Macromolecules* **2007**, *40*, 8695.
75. L. Ghassemzadeh, M. Marrony, R. Barrera, K. D. Kreuer, J. Maier, K. Mu¨ller, *J. Power Sources* **2009**, *186*, 334.
76. M. Schulze, M. Lorenz, N. Wagner, E.Gulzow, Fresenius' *J. Anal. Chem.* **1999**, *365*, 106.
77. M. C. Militello, S. W. Gaarenstroom, *Surf. Sci. Spectra* **2005**, *10*, 117.
78. N. H. Jalani, K. Dunn, R. Datta, *Electrochim. Acta* **2005**, *51*, 553.
79. J. Xie, D. L. Wood, K. L. More, P. Atanassov, R. L. Borup, *J. Electrochem. Soc.* **2005**, *152*, A1011.
80. J. Seo, W. Jang, S. Lee, H. Han, *Polymer Degrad. and Stab.* **2008**, 93, 298
81. L. Wang, B. L. Yi, H.M. Zhang, Y.H. Liu, D.M. Xing, Z.-G. Shao, Y.H Cai, *J. Power Sources* **2007**, *167*, 47-52.
82. C.-H. Wang, H.-Y. Du, Y.-T. Tsai, C.-P. Chen, C.-J. Huang, L.C. Chen, K.H. Chen and H.-C. Shih, *J. Power Sources* **2007**, *171*, 55-62.
83. M. Kawamoto, S. Hitomi, T. Murata, *47th Battery Symposium in Japan preprints* **2006**.
84. H. Nishikawa, S. Hitomi, T. Murata, *47th Battery Symposium in Japan preprints* **2006**.
85. J. H. Wee, K. Y. Lee, S. H. Kim, *J. Power Sources* **2007**, *165*, 667.
86. D. Gruber, N. Ponath, J. Miller, F. Lindstaedtee, K. Y. Lee, S. H. Kim, *J. Power Sources* **2005**, *150*, 67.
87. Y. Shibata, A. Ishihara, S. Mitsujima, N. Kamiya, K. Oota, *47th Battery Symposium in Japan preprints* **2006**.
88. J. Maruyama, A. Okamura, K. Miyazaki, I. Abe, *47th Battery Symposium in Japan preprints* 2006.
89. J. O. Bockris, H. Wroblowa, *J. Electroanal. Chem.* **1959**, *7*, 428.
90. D. Lee, S. Hwang, I. Lee, *J. Power Sources* **2005**, *145*, 147.
91. D. C. Papageorgopoulos, M. Keijzer, F. A. de Bruijn, *Electrochim. Acta* **2002**, *48*, 197.
92. Ioroi, T. Akita, S. Yamazaki, Z. Siroma, N. Fujiwara, K. Yasuda, *Electrochim. Acta* **2006**, *52*, 491.
93. M. Watanabe, S. Motoo, *J. Electroanal. Chem.* **1975**, *60*, 267.
94. H. Fernández, S. Rojas, P. Ocón, J. L. Gómez de la Fuente, P. Terreros, M. A.

Peña, J. L. García-Fierro, *Appl. Catal. B*, **2007**, *77*, 19.
95. N. Travitsky, T. Ripenbein, D. Golodnitsky, Y. Rosenberg, L. Burshtein, E. Peled , *J. Power Sources* **2006**, *161*, 782.
96. S. Kumar, S. Z. Vol, *Electrochem. Commun.* **2006**, *8*, 1151.
97. Yu, M. Pemberton, P. Plasse, *J. Power Sources* **2005**, *144*, 11-20.
98. L. Zhang, K. Lee, J. Zhang, *Electrochim. Acta* **2007**, *52*, 7964.
99. Z. Farhat, A. Alfantazia, *Mater. Sci. Eng.* **2008**, *476*, 169.
100. G. Chen, S. Li, Q. Yuan, *Catal. Today* **2007**, *120*, 63.
101. E. Antolini, J. R. C. Salgado, E. R. Gonzalez, *J. Power Sources* **2006**, *160*, 957.
102. C. A. Vega, I. Fernndez, *Bioelectrochemistry* **1987**, *17*, 217.
103. Int. J. *Hydrogen Energy* **1984**, *9*, 1038.
104. S. J. Lee, S. Mukerjee, J. McBreen, Y. W. Rho, Y. T. Kho, T. H. Lee, *Electrochim. Acta* **1998**, *43*, 3693.
105. C. Wan, M. Lin, Q. Zhuang, C. Lin, *Surf. Coat. Technol.* **2006**, *201*, 214.
106. D. Bevers, N. Wagner, M. V. Bradke, *Int. J. Hydrogen Energy* **1998**, *23*, 57.
107. L. Giorgi, E. Antolini, A. Pozio, E. Passalacqua, *Electrochim. Acta* **1998**, *43*, 3675.
108. T. R. Ralph, G. A. Hards, J. E. Keating, S. A. Campbell, D. P. Wilkinson, M. Davis, J. St-Pierre, M. C. Johnson, *J. Electrochem. Soc.* **1997**, *144*, 3845.
109. M. S. Wilson, S. Gottesfeld, *J. Electrochem. Soc.* **1992** *139*, L28.
110. A. Therdthianwong, P. Manomayidthikarn, S. Therdthianwong, *Energy* **2007**, *32*, 2401.
111. Z. Liu, L. M. Gan, L. Hong, W. Chen, J. Y. Lee, *J. Power Sources* **2005**, *139*, 73.
112. J. Wang, G. Yin, Y. Shao, S. Zhang, Z. Wang, Yunzhi Gao, *J. Power Sources* **2007**, *171*, 331.
113. X. Zhang, W. Jiang, D. Song, J. Liu, F. Li, *Materials Letters* **2008**, *62*, 2343.
114. I. Jang, H. S. Uh, H. J. Cho, W. Lee, J. P. Hong, N. Lee, *Carbon* **2007**, *45*, 3015.
115. P. Gopinath, J. Gore, *Combust. Flame* **2007**, *151*, 542.
116. Z. Liu, X. Y. Ling, B. Guo, L. Hong, J. Y. Lee, *J. Power Sources* **2007**, *167*, 272.
117. K. Jeng, C. Chien, N. Hsu, S. Yen, S. Chiou, S. Lin, W, Huang, *J. Power Sources* **2006**, *160*, 97.
118. Rajalakshmi, H. Ryu, M. M. Shaijumon. S. Ramaprabhu, *J. Power Sources* **2005**, *140*, 250.

Chapter 2 Structural Analysis of a Perfluorosulfonate Ionomer in Solution by ^{19}F and ^{13}C NMR

2.1. Introduction to Chapter 2

The most important development subjects relating to polymer electrolyte fuel cells (PEFC) consist of cost reductions, extending the life of the cells, and improving reliability. As at this point the need for stability in the polymer electrolyte membrane is also significant, the development of a polymer electrolyte membrane offering higher performance, low cost, and long service life is being advanced. The ion exchange membrane of a perfluorosulfonate ionomer is generally used as a polymer membrane that satisfies these requirements. Nafion, Flemion, and Aciplex, with varying grades of ion exchange capacity and film thickness, are among the available marketed products. The catalytic layer in PEFC has a large effect on performance; this catalytic layer is often impregnated with a perfluorosulfonate ionomer solution. In this way, the perfluorosulfonate ionomer fulfills an important role in PEFC. It is therefore necessary to examine the composition and degradation of the perfluorosulfonate ionomer in the research and development of PEFC. In this process, NMR has proven to be one of the most useful analytical tools. The first step in this process entails clarification of the assignment of ^{19}F and ^{13}C NMR in the undegraded article.

To date, three reports have been issued on NMR assignments of perfluorosulfonate ionomers.[1-3] In the report of ref 1, ^{19}F NMR assignment was carried out for Nafion in solution. However, some of the assignments described in that report were corrected by subsequent reports. In refs 2 and 3, ^{19}F and ^{13}C NMR assignments were carried out using the J-modulated ^{13}C CP/MAS technique[2] and solid-state 2D NMR experiments. [3] However, in these reports the separation of two ^{13}C signals (OCF_2) in the side chain is not sufficient to be clearly visible. When the degradation of Nafion is examined using these methods, it may not be possible to clarify the initial point from which degradation progressed.

In this context, we carry out ^{19}F and ^{13}C NMR assignments and structural analysis for Nafion, a perfluorosulfonate ionomer in solution. By solution NMR, we can obtain spectra at satisfactory resolution, permitting detailed examination of the chemical structure. After the membranes of perfluorosulfonate ionomers of differing chemical structures and degraded are dissolved[4,5] using the method described here, structural analysis of the membranes can be carried out. As a side note, it has been reported that

perfluorosulfonate ionomers aggregate in solution.[5-8] In the meantime, according to solution ^{19}F NMR, it was reported that the Nafion solution was true solution and that the aggregates were not found.1 Using solution ^{19}F NMR of high magnetic field, we examine the existence of the aggregates more in detail.

For the structural analysis of perfluorinated organic compounds by ^{19}F and ^{13}C NMR, to date, ^{19}F-^{13}C heteronuclear multiple-quantum coherence (HMQC) and ^{19}F-^{13}C (heteronuclear multiple bond correlation) (HMBC) have been applied.[9-12] However, using the above-mentioned 2D NMR method, assignment of Nafion is impossible due to its chemical structure. We therefore propose new methods to address this issue, referred to as ^{19}F-^{13}C heteronuclear single quantum coherence (HSQC[13,14]) and ^{19}F-^{13}C constant time inverse-detected gradient accordion rescaled long-range heteronuclear multiple bond correlation (CIGAR-HMBC[15]). In experiments using these methods, it is anticipated that correlations for a wider range of $^{2}J_{FC}$ with higher resolution for the ^{13}C axis will be obtained, relative to conventional experiments. Moreover, in addition to use of ^{19}F-^{19}F correlated spectroscopy (COSY),[12,16] we have found that structural analysis for a greater number of perfluorinated organic compounds than previously thought possible is attainable. However, we are hardly able to obtain correlation peaks in 2D NMR of Nafion. We therefore carry out 2D NMR on some model compounds, and the ^{19}F and ^{13}C assignments of these model compounds are determined.

On the basis of the NMR assignments of the model compounds and on ^{19}F coupled and ^{19}F decoupled ^{13}C NMR of Nafion, we determine ^{19}F and ^{13}C NMR assignments of Nafion in solution. We also examine the chemical structure of Nafion using MALDI-MS. Here we discuss the structural analysis of Nafion in solution.

2.2. Experiments

2.2.1. Materials.

Two model compounds, perfluoro(2,5,8-trimethyl-3,6,9-trioxadodecanoyl) fluoride (PFTTF) and perfluoro(2-ethoxyethane)sulfonic acid (PFESA), were purchased from Daikin Fine Chemical Laboratory, Ltd., and from Lancaster Synthesis Inc., respectively. No solvents were added to the PFTTF and PFESA for the NMR experiments. Nafion 5% solution in lower alcohols and water was purchased from Aldrich. The nominal EW (equivalent weight) value is 1100. The solution was used as it is for ^{19}F NMR experiments. For ^{13}C NMR experiments, the solution condensed to approximately 1/4 the volume of the original solution and then diluted with an equal volume of methanol-d_4.

2.2.2. NMR.

NMR spectra were collected using a Varian UNITY INOVA 600 and a Varian UNITY Plus 500 at 25 °C. C_6F_6 was used as an external reference (δ_{19F} = -163 ppm) for ^{19}F chemical shifts. For ^{13}C chemical shifts, TMS was used as an external reference (δ_{13C} = 0.00 ppm).

For the complete fluorine decoupled ^{13}C NMR experiments, WURST[17-19] was employed, and for selective fluorine decoupled ^{13}C NMR experiments, continuous wave was employed.

For PFTTF, HSQC, and the CIGAR-HMBC spectra were obtained at 474 MHz using a 1.0 s relaxation delay, a 13.5 μs ^{19}F $\pi/2$ pulse, a 8.5 μs13C $\pi/2$ pulse, an acquisition time of 0.128s (with ^{13}C GARP decoupling), and coupling constants $^{1}J_{CF}$) 285 Hz for HSQC and $^{1}J_{CF}$) 250-310 Hz and $^{2}J_{CF}$) 30-50 Hz for CIGAR-HMBC, spectral windows of 12,000 Hz for *F*1 and *F*2 axis, 2048 points on *F*2 and 256 points on *F*1 axis, 16 or 128 transients for each *t*1 increment. The *F*2 axis of 12,000Hz was regions of approximately -149 to -127 ppm and -96 to -74 ppm, and HSQC and CIGAR-HMBC were carried out in the two regions, respectively.

The COSY spectrum for PFTTF was collected at 564 MHz using spectral windows of 50,000 Hz, 8192 points on the *F*2 and 256 points on the *F*1 axis, a 3.0 s relaxation delay, and a 5.8 μs 19F π/2 pulse. For each *t*1 increment four transients were produced. All 2D NMR were of the gradient-selected type.

The conditions of the HSQC, CIGAR-HMBC, and COSY experiments for PFESA were approximately the same as those for PFTTF.

All data were processed using Varian's VNMR software. The HSQC data were processed with a Gaussian weighting function and zero filled to 4-fold in the *F*1 dimension. The CIGAR-HMBC and COSY data were processed with a sinebell weighting function and zero filled to 4-fold in the number of points collected on the *F*1 axis.

2.2.3. MALDI-MS.

A sample solution was prepared by diluting the commercial Nafion solution in 2,2,2-trifluoroethanol (20 mg/mL). Matrix solution was prepared by dissolving the 7-amino-4-methylcoumarin in 2,2,2-trifluoroethanol (10 mg/mL). The two solutions were mixed in a 1:1 ratio by volume. 2 μL of the mixed solution was dropped onto the sample plate and air-dried. MALDI-MS measurements were performed with a Bruker BIFLEX III time-of-flight mass spectrometer. The instrument operates with a nitrogen laser providing 3 ns pulses at 337 nm. Negative ions were detected in the reflectron mode.

2.3. Results

2.3.1. Model Compounds.

As model compounds, perfluoro(2,5,8-trimethyl-3,6,9-trioxadodecanoyl) fluoride (PFTTF) and perfluoro(2-ethoxyethane)sulfonic acid (PFESA) were used, the chemical structures of whichare shown in Table 1. Each compound contains -OCF_2-$CF(CF_3)O$- or -$OCF_2CF_2SO_3H$ as a part of its chemical structure. Since each substructure corresponds partially to the structure of the Nafion side chain, therefore, PFTTF and PFESA may be deemed suitable as model compounds.

Table 2-1. Chemical Structure of Model Compounds (PFTTF, PFESA) and Nafion

PFTTF	Perfluoro(2,5,8-trimethyl-3,6,9-trioxadodecanoyl)fluoride
	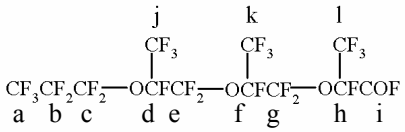
PFESA	Perfluoro(2-ethoxyethane) sulfonic acid
	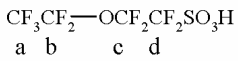
Nafion	Nafion for the acid form
	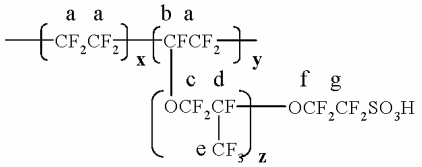

2.3.1.1. Assignments of PFTTF.

In the chemical structure shown in Table 1, the suffixes a to j are attached to each CF_n. For example, “Fa” and “Ca” represent the fluorine and the carbon with “a” attached, espectively. The ^{19}F NMR spectrum and ^{19}F decoupled ^{13}C NMR spectrum of PFTTF are shown in Figure 1 and Figure 2, respectively. The complete assignments are summarized in Table 2. The reasons for each assignment are described as follows.

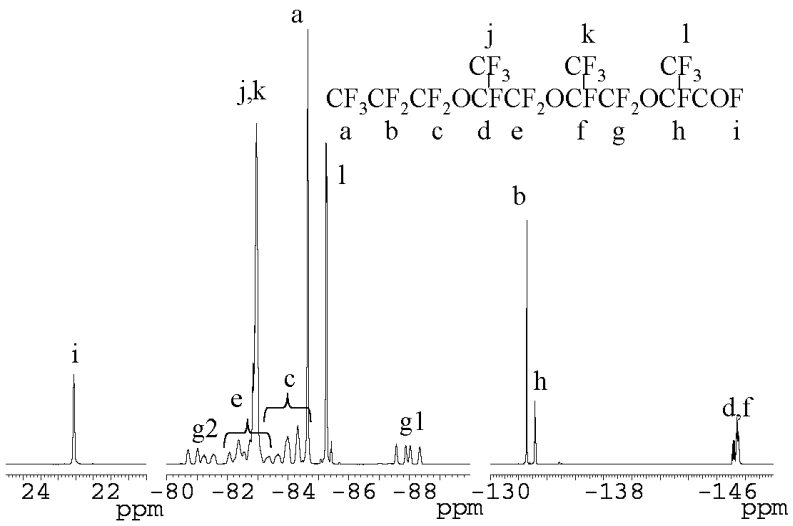

Figure 2-1. ^{19}F NMR spectrum of PFTTF.

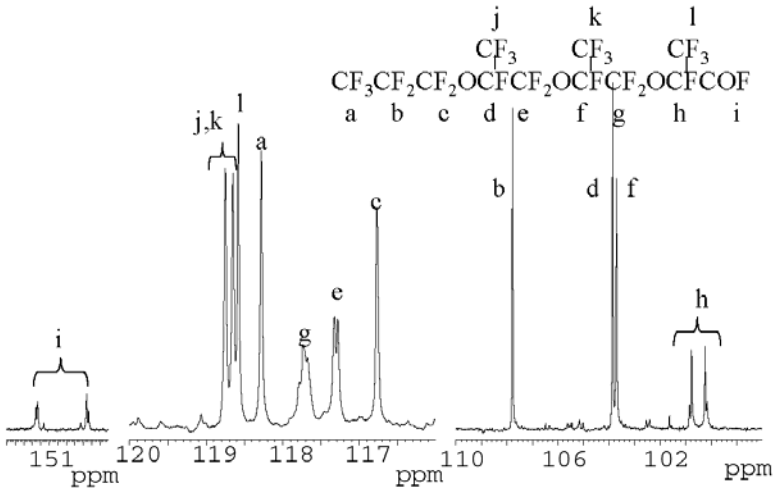

Figure 2-2. ^{19}F complete decoupled ^{13}C NMR spectrum of PFTTF.

Scheme 2-1

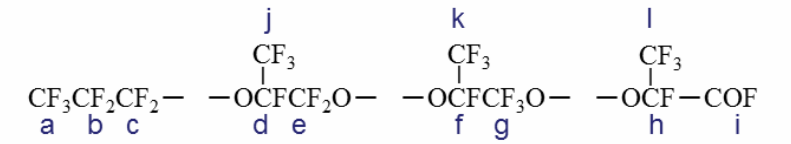

Table 2-2. ^{13}C, ^{19}F NMR Assignment and $^{1}J_{CF}$, $^{2}J_{CF}$ of PFTTF

	^{19}F chemical shifts (ppm)	^{13}C chemical shifts (ppm)	$^{1}J_{CF}$(Hz)	$^{2}J_{CF}$(Hz)	multiplicity of ^{13}C peaks
a	-84.7	118.3	284	33	q, t
b	-132.6	107.8	271	40	t, s
c	-85～-83	116.8	289	31	t, t
d	-147.7～-147.1	103.9	269	37	d, s
e	-84～-82	117.3	287	29	t, d
f	-147.7～-147.3	103.7	270	36	d, s
g	-88.0, -81.2	117.7	289	26	t, d
h	-133.2	100.5	262	41	d, q, d
i	23.1	149.7	372	37	d, d
j ,k	-83.0	118.65,118.75	287	31	q, d
l	-85.3	118.6	285	29	q, d

* q : quartet, t : triplet
s : sextet, d:doublet

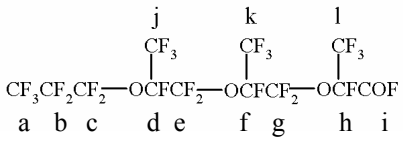

The ^{13}C peaks of 149.7 and 100.5 ppm, which are not completely ^{19}F decoupled in Figure 2, are assigned to Ci and Ch, respectively. Fi is assigned to 23.1 ppm on the basis of the chemical shift value.20 Since the chemical shift of Fi differs significantly from that of other fluorines, Fi is not completely decoupled in Figure 2.

The chemical structure of PFTTF is then divided into four perfluorocarbon substructures, as shown in Scheme1, and these perfluorocarbons are assigned by HSQC and CIGAR-HMBC of PFTTF (Figure 3 and Figure 4). In HSQC and CIGAR-HMBC spectra, correlation peaks via $^{1}J_{FC}$ and $^{2}J_{FC}$, respectively, are yielded. As a result, the ^{19}F and ^{13}C assignments are determined for four substructures. To connect these four substructures, we apply ^{19}F-^{19}F COSY. ^{19}F-^{19}F COSY yields correlations between fluorine peaks via $^{2}J_{FF}$, $^{3}J_{FF}$, $^{4}J_{FF,}$ and $^{5}J_{FF}$.[12,16] In Figure 5 for COSY, the correlations caused by $^{4}J_{FF}$ are identified (Fc-Fd, Fe-Ff, and Fg-Fh). The methods of identification are as follows. The correlations via $^{2}J_{FF}$ are identified by HSQC, and the correlations via $^{3}J_{FF}$ are identified by HSQC and CIGAR-HMBC. The remaining correlations in COSY are identified via $^{4}J_{FF}$. No correlations via $^{5}J_{FF}$ are observed. The ^{19}F and ^{13}C NMR assignments of PFTTF are thus completed. The assignments of the ^{13}C peaks are supported by the multiplicity of carbon peaks in the ^{19}F coupled ^{13}C NMR spectrum.

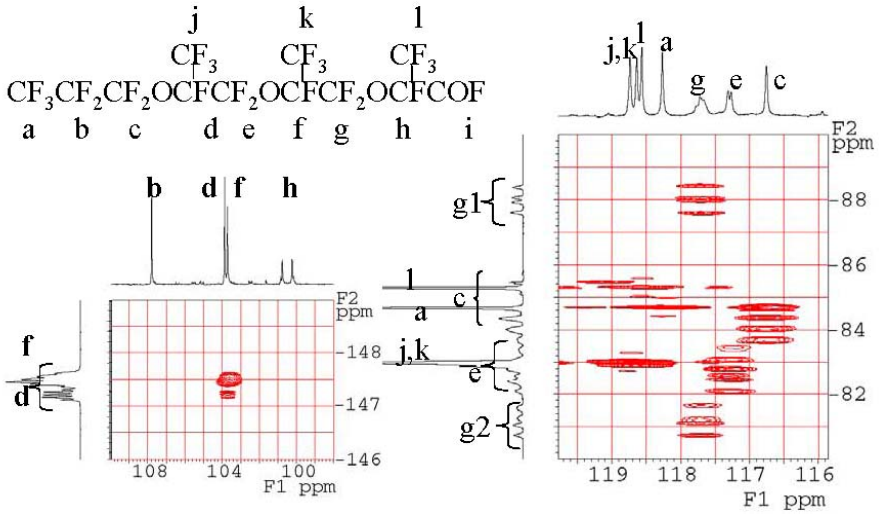

Figure 2-3. (a) ^{19}F-^{13}C HSQC spectrum of PFTTF. (b) ^{19}F-^{13}C HSQC spectrum of PFTTF.

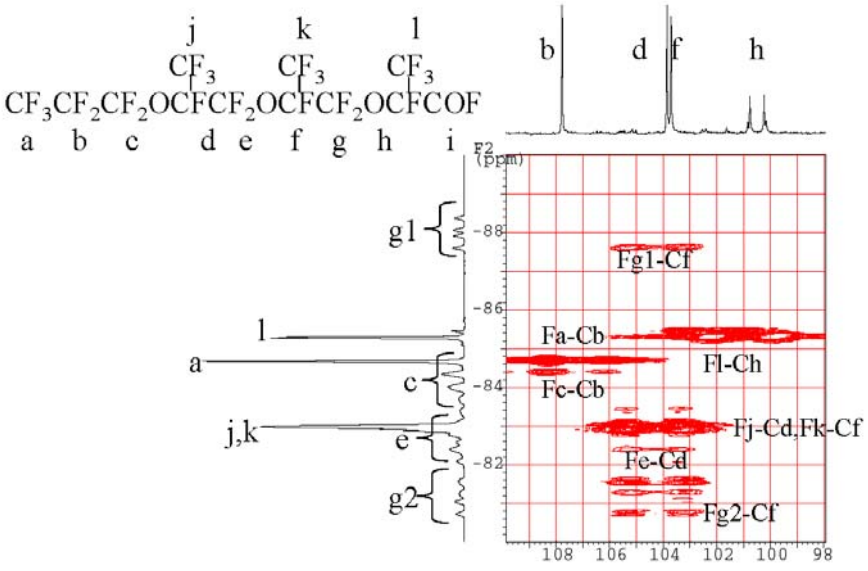

Figure 2-4. ^{19}F-^{13}C CIGAR-HMBC spectrum of PFTTF.

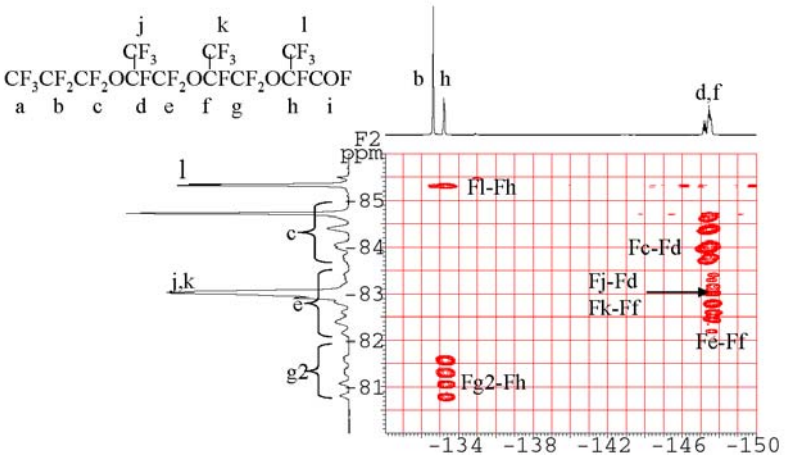

Figure 2-5. ^{19}F-^{19}F COSY spectrum of PFTTF.

2.3.1.2. Assignments of PFESA.

In the chemical structure shown in Table 1, the suffixes a to d are attached to each CF_n. Figure 6 shows the ^{19}F and ^{13}C NMR spectra of PFESA. Applying the same method used with PFTTF, we determine complete assignments. The assignments are summarized in Table 3.

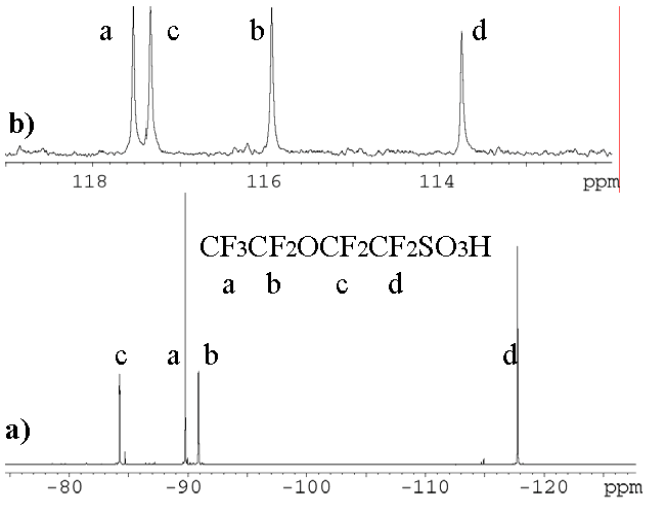

Figure 2-6. (a) ^{19}F NMR spectrum of PFESA. (b) ^{13}C NMR spectrum of PFESA.

Table 2-3. ^{13}C, ^{19}F NMR Assignment and $^{1}J_{CF}$, $^{2}J_{CF}$ of PFESA

	^{19}F chemical shifts (ppm)	^{13}C chemical shifts (ppm)	$^{1}J_{CF}$(Hz)	$^{2}J_{CF}$(Hz)	multiplicity of ^{13}C peaks
a	-89.7	117.5	283	42	q, t*1
b	-90.9	116.0	286	46	t, q*1
c	-84.2	117.4	288	30	t, t*1
d	-117.7	113.8	298	36	t, t*1

*1 q : quartet, t : triplet

$CF_3CF_2OCF_2CF_2SO_3H$
a b c d

2.3.2. Structure Analysis of Nafion.

In Table 1, the suffixes a to g are attached to each CF_n in the chemical structure, with the numbers of the repeating unit represent as x and y.

2.3.2.1. Assignment of ^{13}C NMR.

^{19}F coupled and ^{19}F complete decoupled ^{13}C NMR spectra are shown in Figure 7. Each ^{13}C peak is assigned using the following two methods. The first method is based on the chemical shift of the model compounds. We assign the $-OCF_2-CF(CF_3)O-$ component in the side chain of Nafion on the basis of the assignments of PFTTF. For the $-OCF_2-CF_2-SO_3H$ component, assignment is made with reference to the assignments of PFESA. The second method is based on spin couplings between ^{19}F and ^{13}C. In the ^{19}F coupled ^{13}C spectrum, ^{13}C peaks give rise to resolved lines mainly by one-bond and two-bond ^{19}F-^{13}C couplings. Because the number of resolved lines depends on the number of ^{19}F atoms that are coupled with the ^{13}C atoms, we can assign ^{13}C peaks. $^{1}J_{FC}$ is normally near 200-400 Hz, and $^{2}J_{FC}$ is near 20-50 Hz.

The 104.0 and 113.5 ppm carbon resonances are identified as Cd and Cg, with reference to the chemical shifts of the model compounds. The assignments of Cd and Cg are supported by the ^{19}F coupled ^{13}C spectrum.

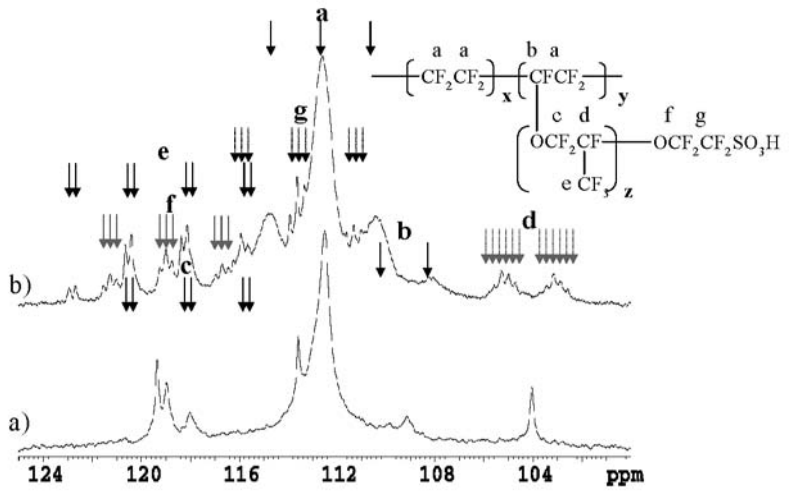

Figure 2-7. ^{13}C NMR spectrum of Nafion: (a) ^{19}F complete decoupled; (b) ^{19}F coupled.

From the ^{13}C chemical shifts of the model compounds, Cc, Ce, and Cf are assigned to 118.0, 119.0, or 119.4ppm. We identify Ce, Cf, and Cc on the basis of the multiplicity of the ^{19}F coupled ^{13}C spectrum. This is because the ^{13}C chemical shifts of the model compounds are closely situated, and it is thus dangerous to assign the three carbons only on the basis of the chemical shifts of the model compounds. Ce is assigned to 119.4 ppm because the peak of 119.4 ppm presents a doublet of quartets. Cf is then assigned to 119.0 ppm, since the peak of 119.0 ppm presents a triplet of triplets. The remaining Cc can be assign to 118.0 ppm. Cc shows a triplet at $^1J_{CF}$, and it overlaps with the Ce peak of the quartet at $^1J_{CF}$ in Figure 7b. There is no contradiction to the assignment of Cc.

Moreover, Ca of the CF_2 in the main chain is assigned to 112.5 ppm. The Ca chemical shift and the multiplicity are also appropriate. Cb, which is CF in the main chain, was assigned to 109.2 ppm and presents a doublet at $^1J_{CF}$ in ^{19}F coupled ^{13}C NMR. All ^{13}C assignments and spin coupling constants are listed in Table 4.

Table 2-4. ^{13}C NMR Assignment of Nafion

	Nafion						Model compounds (ppm)
	CF, CF_2, CF_3 *1	previous work (ppm) *2	this work (ppm)	multiplicity	$^1J_{CF}$, $^2J_{CF}$ (Hz)	line width (Hz)	
a	CF_2	111.3 to 111.8	112.5	t	290 *3	97	-
b	CF	108.1	109.2	d	265 *3	92	-
c	CF_2	116.7	118	t-d	- *4	75	118.0 or 118.4 *5
d	CF	102.9	104	d-s	267, 37	27	104.4 or 104.5 *5
e	CF_3	117.9	119.4	q-d	287, 32	30	119.3 or 119.4 *5
f	CF_2	117	119	t-t	291, 34	51	117.4 *6
g	CF_2	112.2	113.5	t-t	290, 37	22	113.8 *6

*1 by ref. 2

*2 by ref. 3

*3 $^1J_{CF}$ is clear, and $^2J_{CF}$ is not clear.

*4 $^1J_{CF}$ and $^2J_{CF}$ are not clear.

*5 chemical shift of PFTTF

*6 chemical shift of PFESA

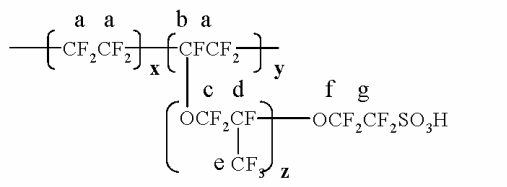

2.3.2.2. Assignment of ^{19}F NMR.

The ^{19}F NMR spectrum of Nafion is given in Figure 8. We assign Fc, Fd, Fe, Ff, and Fg peaks in the side chain of Nafion with reference to the chemical shifts of the model compounds (Tables 2 and 3). The remaining peaks are assigned to CF (Fb) and CF_2 (Fa) in the main chain. The larger peak of -123.2 ppm is assigned to CF_2 (Fa), and the smaller one of -140.1 ppm is assigned to CF (Fb). ^{19}F assignments of Nafion are listed in Table 5. This table includes the ^{19}F chemical shifts of the model compounds. All ^{19}F assignments are confirmed by ^{19}F single frequency decoupled ^{13}C NMR experiments. The line shape of the skirt of the Fg peak is not symmetrical. From the chemical shift, both neighbors CF_2 of the Fb may be obtained here; both overlap the Fg peak.

The integrated values of ^{19}F NMR peaks are shown in Table 6.

2.3.2.3 MALDI-MS.

The MALDI-MS spectrum of Nafion is shown in Figure 9. The main peaks are obtained in the *m*/*z* range between 1302 and 3078. It is assumed that the low molecular weight component is the result of selective ionization, since the molecular weight of Nafion in solution should be much higher. This type of phenomenon is frequently seen

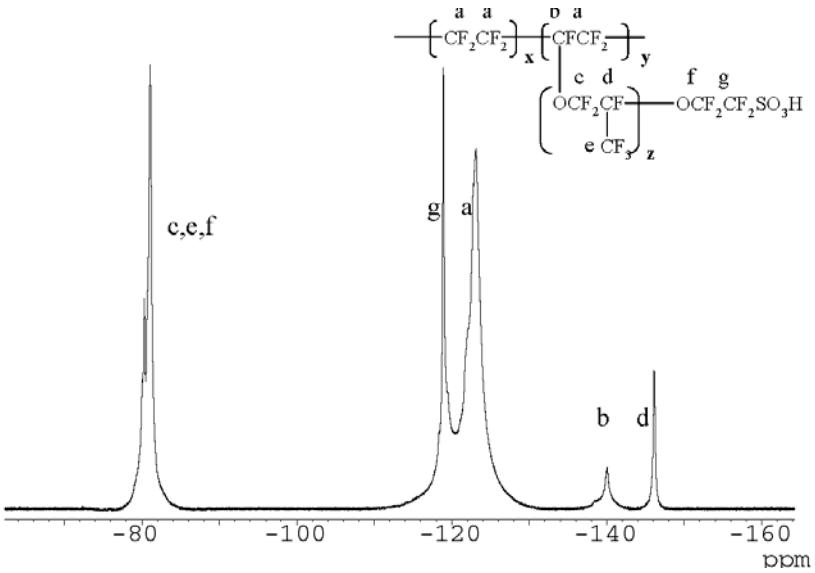

Figure 2-8. ^{19}F NMR spectrum of Nafion.

Table 2-5. ^{19}F NMR Assignment of Nafion

	Nafion				Model compounds (ppm)
	previous work (ppm)*1	previous work (ppm)*2	this work (ppm)	line width (Hz)	
a	-120	-122.1 to -118.2	-123.2	780	-
b	-	-138.4	-140.1	317	-
c	-80	-80.1	-80.3, -80.1	-*3	-84 to -82*4
d	-146	-143.8	-146.1	153	-147.7 to -147.1*4
e	-80	-80.4	-80.3, -80.1	-*3	-332
f	-80	-79.9	-80.3, -80.1	-*3	-421
g	-139	-117.1	-118.9	134	-588.5

*1 by ref. 1

*2 by ref. 3

*3 line width is not clear.

*4 chemical shift of PFTTF

*5 chemical shift of PFESA

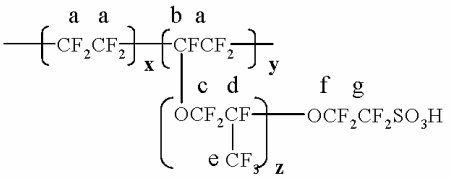

in MALDI-MS of polymers with wide molecular weight distribution. The main peaks are observed every 444 Da, which corresponds to $C_7HF_{13}O_5S$. Consequently, it is estimated that the principal structure in the side chain was -O-CF_2CF-(CF_3)-O-CF_2CF_2-SO_3H. This substructure agrees with that estimated by NMR.

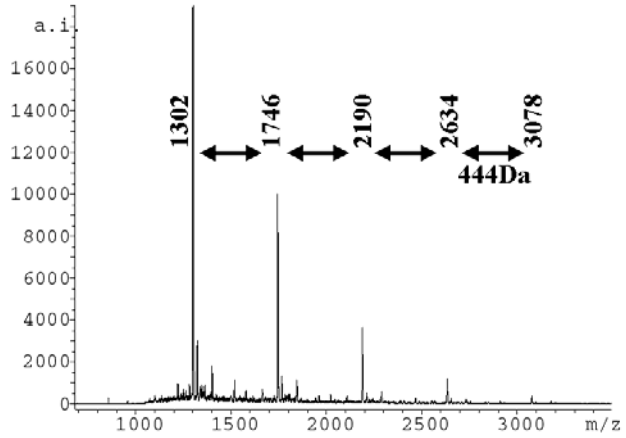

Figure 2-9. MALDI-MS spectrum of Nafion

Table 2-6. Integrated Values of ^{19}F NMR of Nafion

^{19}F peak	Fc, Fe, Ff	Fa, Fg	Fb	Fd
Solution NMR: A	6.94	19.70	0.88	1.00
Solid-state NMR: B[*1]	7.00	25.90	0.90	1.00
A/B	0.99	0.76	0.98	1.00

*1 by ref. 3

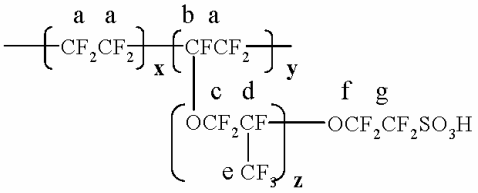

2.4. Discussion

We perform ^{19}F and ^{13}C NMR assignments of the model compounds of a perfluorosulfonate ionomer using HSQC, CIGAR-HMBC, and COSY. This represents a

new approach to the structural analysis of perfluorinated organic compounds. This approach is applicable to structural analysis of a much greater number of perfluorinated organic compounds than previously thought possible.

^{19}F and ^{13}C NMR assignments for Nafion in previous reports1,3 are also listed in Tables 5 and 4. Our ^{19}F and ^{13}C assignments agree with ref 2 and ref 3, thus confirming these assignments. In our ^{13}C NMR, the two OCF_2 (Cc, Cf) in the side chain are observed to be more clearly resolved. This is because line widths using solution NMR are little smaller than those using solidstate NMR. The respective line widths for Cc and Cf are 0.4 and 0.6 ppm by solution NMR and 0.5 and 1.1 ppm by solid-state NMR.[3]

Table 6 shows the integrated values ^{19}F peaks by solution NMR and by solid-state NMR[3] for Nafion of EW 1100. Here, we assume that the integrated value of the Fd peak is 1.00. The total integrated value of Fc, Fe, and Ff peaks by solution NMR agrees with that by solidstate NMR. That is to say, in the side chain, integrated value by solution NMR agrees with that by solid-state NMR. On the other hand, the integrated value of Fa by solution NMR is smaller than that by solid-state NMR. The integrated value of Fa alone is not obtained in practice by solution NMR because Fa and Fg have not separated. However, as Fg is small, its effect can be disregarded. As this result, in solution NMR, it is proven that over 20% of CF_2 in the main chain is not detected in comparison with solid-state NMR. These phenomena suggest the presence of aggregates in Nafion solution and are explained as follows. Some of the main chains gather inside the aggregates, reducing their mobility, so we are not able to detect them by solution NMR. The side chain is present on the surface of the aggregates, with mobility approximately equivalent to that of the solution state. Moreover, using the line widths of ^{19}F solution NMR, we can also estimate the state of the aggregates. The line width of Fg is the smallest among those in the side chain, and the mobility near the sulfonate group is especially high in the side chain. Specifically, this suggests that the aggregates are pointing their sulfonate groups outward. So far, some reports indicated the presence of aggregates in the Nafion solution, through the use of dynamic light scattering,[6] neutron scattering, and X-ray scattering.[7,8] The state of the aggregates suggested here agrees with that in ref 7. In another issue,[1] it was reported that Nafion solution in ethanol was a true solution and that aggregates were undetectable using solution NMR. This contradicts our results. For the Nafion solution at least used here is considered to contain the aggregates, for the following three reasons. (1) In ref 1, there are some errors in the assignments. (2) The magnetic field of the NMR instrument used in ref 1 is low, and the peak separation and signal-to-noise ratio are insufficient. Therefore, this does not seem to indicate an accurate integrated value. (3) The solvent composition of

the Nafion solution used in this report does not agree with that in ref 1. The state of the aggregates also changes depending on the solvent compositions[6] and other conditions. The higher-order structures and the physical characteristics of the polymer in catalysis layer in PEFC are greatly influenced by the states of the aggregates in the polymer solution used as the raw material. For these reasons, the evaluation of aggregates provides interesting results.

At first we carried out 2D NMR experiments on Nafion in solution, but we had difficulty obtaining correlation peaks, for the following reasons. The line widths of the ^{19}F peaks in the main chain are very broad, at 300-800 Hz. On the other hand, those of the model compounds are less than 80 Hz. It is well-known that T_2 (transverse relaxation time) generally decreases with increasing line width. This indicates that the T_2 of Nafion is considerably shorter than that of normal perfluorinated organic compounds. It is concluded that magnetization is attenuated for the pulse train of 2D NMR and that the correlation signals cannot be obtained.

It is known that the chemical structures of the perfluorosulfonate ionomers differ by manufacturing company and by type. To elucidate the degradation mechanism and development of a polymer with high durability, it is necessary to examine the chemical structures in detail. Using the assignment method we have presented, it becomes possible to clarify slight differences in chemical structure and the position at which degradation occurs. However, the attention is needed, because the integrated value of CF_2 in the main chain by solution NMR is smaller than practice. Therefore, it is considered that solution NMR is suitable for examining the detailed structure of the side chain of perfluorosulfonate ionomers. To examine the main chain and the whole structure of perfluorosulfonate ionomers, solid-state NMR is appropriate. Moreover, using solution NMR, since information on aggregates in polymer solution is also suggested, significant contributions to research and development of PEFC become possible.

2.5. Conclusion

1. We apply ^{19}F-^{13}C HSQC, ^{19}F-^{13}C CIGAR-HMBC, and ^{19}F-^{19}F COSY to model compounds of a perfluorosulfonate ionomer, and we determine all ^{19}F and ^{13}C assignments. This represents a new approach to the structural analysis of perfluorinated organic compounds.

2. On the basis of the ^{19}F and ^{13}C assignments of the model compounds and based on

the analysis of spin couplings between ^{19}F and ^{13}C of a perfluorosulfonate ionomer, we clearly determine all ^{19}F and ^{13}C assignments of the perfluorosulfonate ionomer. Our assignments agree with those in ref 3, thus confirming the reported assignments of ^{19}F and ^{13}C NMR. In our ^{13}C NMR of the perfluorosulfonate ionomer in solution, two OCF_2 in the side chain are observed as more clearly separated.

3. We clarify the structure of a perfluorosulfonate ionomer in solution by NMR. Results of MALDI-MS support those of NMR.

4. On the basis of the NMR assignments and the integrated values, the presence of aggregates in a perfluorosulfonate ionomer solution is suggested. It is estimated that the aggregates are pointing their sulfonate groups outward and that some of the main chains gather inside the aggregates.

2.6. Acknowledgment.

We thank Mr. Yoshikatsu Nagasawa for his useful suggestion on this work.

2.7. Supporting Information

HSQC, CIGAR-HMBC, and COSY of PFESA; ^{19}F selective decoupled ^{13}C NMR of Nafion.

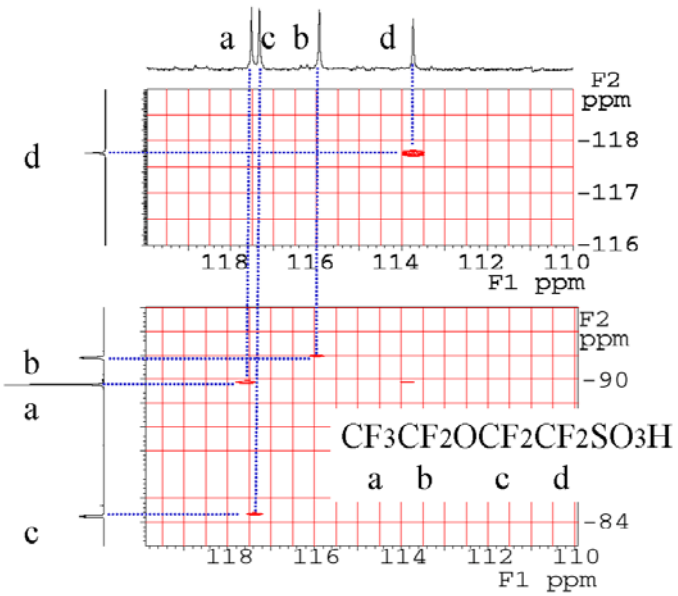

Figure SI2-1. ^{19}F-^{13}C HSQC spectrum of PFESA

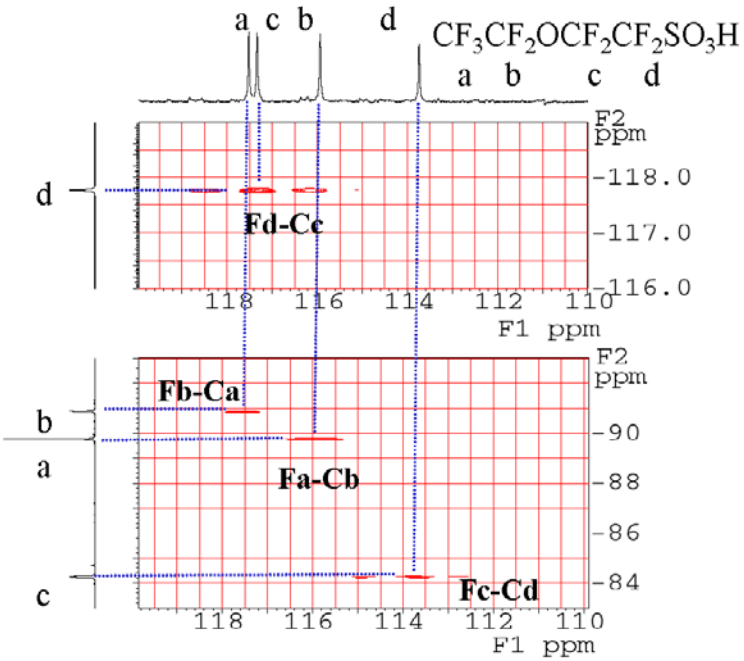

Figure SI2-2. ^{19}F-^{13}C CIGAR-HMBC spectrum of PFESA

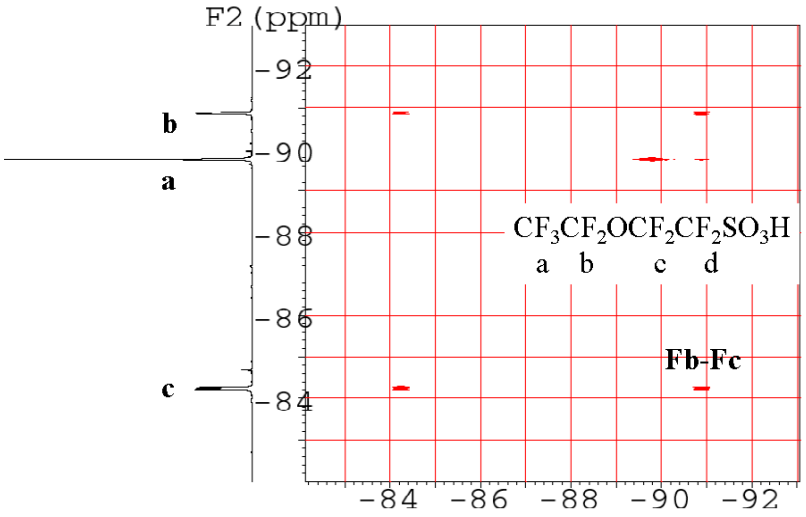

Figure SI2-3. ^{19}F- ^{19}F COSY spectrum of PFESA

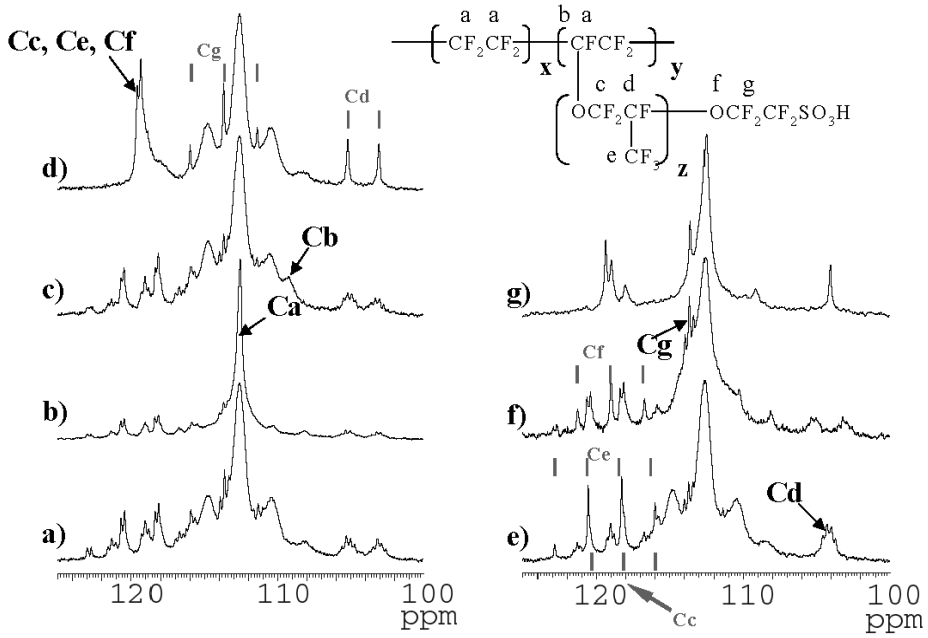

Figure SI2-4. ^{19}F coupled, ^{19}F Single frequency decoupled and ^{19}F complete decoupled ^{13}C NMR spectrum of Nafion™ a) ^{19}F coupled, b) Fa selective decoupled, c) Fb selective decoupled, d) Fc,Fe and Ff selective decoupled, e) Fd selective decoupled, f) Fg decoupled and g) ^{19}F complete decoupled.

2.8. References of chapter 2.

1. S.Schlick, G. Gebel, M. Pineri, F. Volino, *Macromolecules* **1991**, *24*, 3517.
2. S.-F. Liu, K. Schmidt-Rohr, *Macromolecules* **2001**, *34*, 8416.
3. Q. Chen, K. Schmidt-Rohr, *Macromolecules* **2004**, *37*, 5995.
4. C. R. Martin, T. A. Rhoades, J. A. Fergason, *Anal. Chem.* **1982**, *54*, 1639.
5. W. G. Grot, C. Ford, European Patent 0066369, 1982.
6. P. A. Cirkel, T. Okada, S. Kinugasa, *Macromolecules 1999*, *32*, 531.
7. P. Aldebert, B. Dreyfus, G. Gebel, N. Nakamura, M. Pineri, F. Volino, *J. Phys. (Paris)* **1988**, *49*, 2101.
8. B. Loppinet, G. Gebel, C. E. Williams, *J. Phys. Chem. B* **1997**, *101*, 1884.
9. M. Bourdonneau, C. Brevard, *Inorg. Chem.* **1990**, *29*, 3270.
10. S. Berger, *J. Fluorine Chem.* **1995**, *72*, 114.
11. A. A. Ribeiro, *Magn. Reson. Chem.* **1997**, *35*, 215.
12. A. A. Ribeiro, *J. Fluorine Chem.* **1997**, *83*, 61.
13. G. Bodenhausen, D. Ruben, *Chem. Phys. Lett.* **1980**, *69*, 185.
14. L. E. Kay, P. Keifer, T. Saarinen, *J. Am. Chem. Soc.* **1992**, *114*, 10663.
15. C. E. Hadden, G. E. Martin, V. V. Krishnamurthy, *Magn. Reson. Chem.* **2000**, *38*, 143.
16. S. Yonemori, H. Sasakura, *J. Fluorine Chem.* **1995**, *75*, 151.
17. E. Kupce, R. Freeman, *J. Magn. Reson., Ser. A* **1995**, *115*, 273.
18. E. Kupce, R. Freeman, *J. Magn. Reson., Ser. A* **1995**, *117*, 246.
19. E. Kupce, R. Freeman, *J. Magn. Reson., Ser. A* **1996**, *118*, 299.
20. E. G. Brame Jr., *Anal. Chem.* **1962**, *34*, 591.

Chapter 3 Degradation Study of Perfluorosulfonic Acid Polymer Electrolyte; Approach from Decomposition Product Analysis

3.1. Introduction to Chapter 3

As part of efforts aimed at the commercialization of proton exchange membrane fuel cells (PEMFC), the development of electrolyte membranes and electrode ionomers with sufficient durability to operate in conditions of low humidity and high temperature has recently attracted interest. It is widely understood that the degradation of a perfluorosulfonic acid (PFSA) polymer electrolyte is accompanied by the emission of fluoride ions,[1-9] and that the chemical stability of the polymer electrolyte is commonly evaluated by the fluoride ion release rate (FRR). However, certain decomposition products other than fluoride ions constitute a significant volume of the product and cannot be ignored when evaluating the degradation of PFSA polymers. In past studies, six kinds of side-chain fragments as decomposition products were identified by means of ^{19}F NMR and MS,[10-12] and PFSA degradation was reported using ^{19}F NMR.[13-19] To date, however, no study has yet reported the quantification of side-chain fragments.

Here, we report a degradation study of PFSA polymer electrolytes based on decomposition product analysis performed mainly by 19F NMR. In particular, quantitative analysis of decomposition products of PFSA polymers in electrodes (catalyst layers) was performed after open circuit voltage (OCV)-hold tests and load cycling tests. Moreover, the durability of conventional and chemically stabilized PFSA polymer electrolyte membranes was examined based on hydrogen peroxide vapor (HPV) exposure tests by means of ion chromatography, total organic carbon analysis and NMR. The differences between the results of fluoride ion release rate (FRR) measurement and decomposition product analysis are discussed.

3.2. Experimental

3.2.1. Fuel cell operation (OCV-hold and load cycling) test

Nafion® 112 membranes having GDL and catalyst layers with Pt catalyst and Nafion® of equivalent weight (EW) 1100 for the electrode were set into a single cell with an effective area of 3 cm × 15 cm, using straight gas channels and a counter flow configuration. An OCV-hold test and a load cycling test (current density: 0.3 A/cm^2 (60 s) ↔ 0.01 A/cm^2 (60 s)) were carried out at a cell temperature of 80 ºC and a humidifier

temperature of 70 ºC with hydrogen/air utilization of 70%/40%. Each test was terminated when the cross-leak current reached 10-20 mA/cm^2.

3.2.2. Hydrogen peroxide vapor (HPV) exposure tests [20]

Conventional (Nafion® 112) and chemically stabilized (Nafion® NRE-212) PFSA polymer electrolyte membranes were exposed to HPV in the apparatus depicted in Figure 1 for 100 hours at controlled temperature and humidity. The exposure atmosphere was 90 ºC (relative humidity (RH): 100%, 70%, and 30%) and 100 ºC (30% RH).

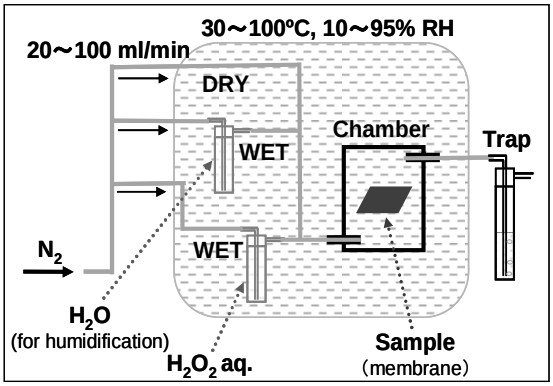

Figure 3-1. Schematic illustration of the HPV exposure test

3.2.3. Decomposition product analysis

3.2.3.1. Fuel cell operation tests

After the tests, the catalyst layers, containing catalyst, carbon and PFSA polymer, were carefully scraped off from the MEAs with a spatula. The weights of the catalyst layers were measured, and used for calculation of the weight % of decomposition products. The catalyst layers were then immersed in water to obtain water extracts. Next, the water extraction residues were immersed in methanol to obtain methanol extracts. Water and propanol were then added to the residues after two extraction stages, and they were placed under 200 ºC at a high pressure for one hour. Thus the last residual PFSA polymer was dissolved in the solvent.

The decomposition products in the water and methanol extracts and the PFSA polymer in the methanol extracts and the dissolved extraction residues were evaluated via ^{19}F NMR (INOVA500, Varian Inc.) with an external reference.[21] The chemical structures of the decomposition products in the water and the methanol extracts were identified according to references. [10-12] Pentafluorophenol with a known concentration

in a coaxial NMR tube was used as a chemical shift reference and reference standard of quantitative analysis for ^{19}F NMR. The weight of PFSA polymer and relative equivalent weight (EW*) were calculated with the areas of ^{19}F NMR signals, according to the signal assignments of references. [22, 23]

The fluoride ion concentration in the drain water for each test was also quantified by ion chromatography (ICS 3000, Dionex Corp.).

3.2.3.2. HPV exposure tests

For the trap water, the concentrations of fluoride, trifluoroacetic acid (TFA) and sulfuric acid ions were investigated via ion chromatography (ICS 3000, Dionex Corp.). Total organic carbon (TOC) was obtained using a total organic analyzer (Shimadzu Corp.).

The membranes were weighed before and after the test. To 200 mg of membranes, a mixture of water and methanol was added, and the solvent extracts were obtained and analyzed. The chemical structures and amounts of decomposition products in the extracts were determined via ^{19}F NMR as mentioned above. The amounts of side-chain fragments obtained from the reference membranes were subtracted from those obtained from the membranes after HPV exposure tests.

3.3. Results and discussion

3.3.1. Degradation of PFSA polymer in PEMFC operation tests

Figure 2 shows plots for FRR and cell voltage as a function of operation time in OCV-hold and load cycling tests. The following three characteristics of the OCV-hold test results are observed. 1) FRR is high from the beginning of the test. 2) Operation time at which the leak current reaches its limit around 850 hours. 3) Cell voltage gradually drops during the test. On the other hand, the features of the load cycling test are as follows. 1) Cathode FRR is initially high, and soon decreases. Anode FRR is initially much smaller, and soon decreases to the detection limit. 2) Operation time is around 2800 hours. 3) Cell voltage remains above 0.83 V until the end of the test. The OCV-hold test shows higher FRR, indicating a higher degradation rate for the PFSA polymer.

^{19}F NMR spectrum of the water extract from the anode catalyst layer after the load cycling test is shown in Figure 3. On reference to the literature [10-12], six kinds of side-chain fragments can be identified in Figure 3, as summarized in Table I. Similarly, these six kinds of side-chain fragments are also obtained from other water extracts.

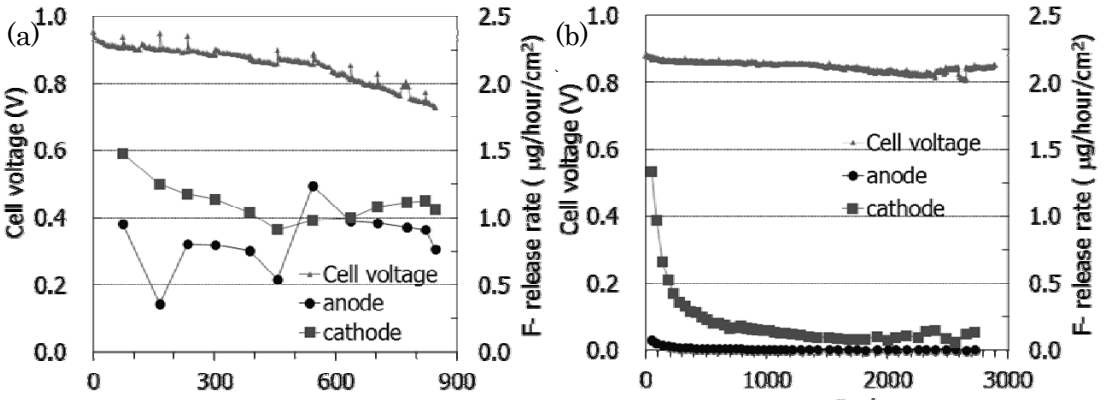

Figure 3-2. FRR and cell voltage vs. time of operation in OCV-hold (a) and load cycling (b) tests. The tests were terminated when the leak current reached the limit (10-20mA).

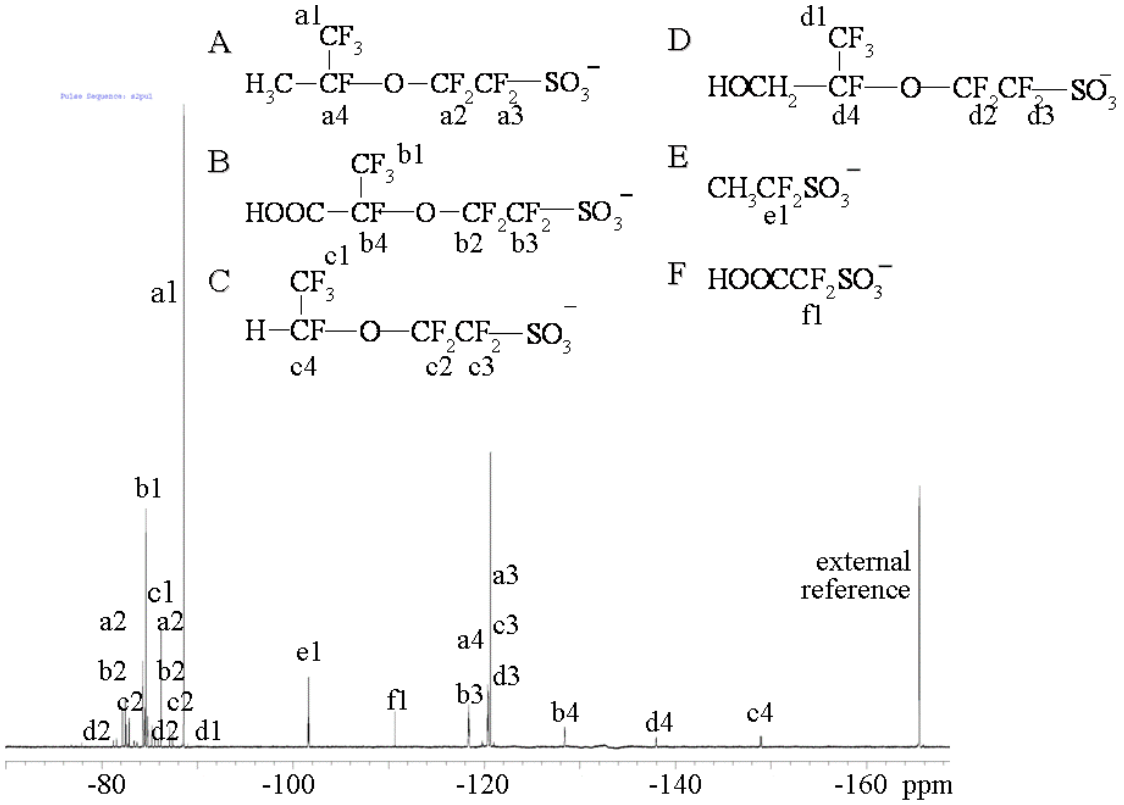

Figure 3-3. ^{19}F NMR spectrum of water extract from the anode catalyst layer after the load cycling test. The chemical structures of the side-chain fragments were quoted from references. [10-12]

Table 3-I. Chemical structures of side-chain fragments [10-12] investigated in extracts from catalyst layers after OCV-hold and load cycling tests.

A	B	C
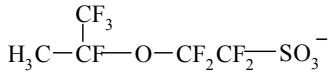	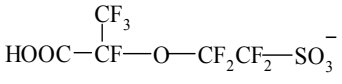	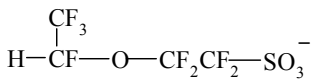
D	**E**	**F (assumed)**
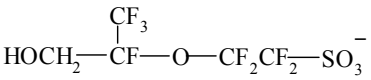	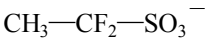	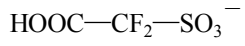

The side-chain fragments indicate that scission occurs at two positions in the side-chain, as shown below.

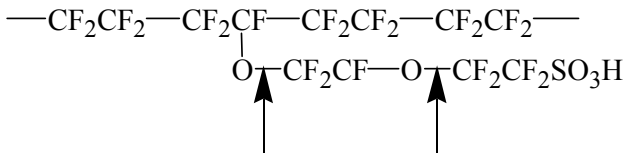

As mentioned below, the side-chain fragments of B and D were also confirmed in the PFSA membranes after the HPV exposure test. It is therefore presumed that generation of the side chain fragments of B and D is related to hydrogen peroxide.

Figure 4 shows the amounts of decomposition products exhausted by the OCV-hold and load cycling tests. The amounts were acquired via ^{19}F NMR. Since PFSA polymer cannot fully swell with water, some of the decomposition products are confined within the PFSA polymer and not extracted into water. In contrast, it swells with methanol, releasing all decomposition products into the methanol. The side-chain fragments in the water extracts and methanol extracts were totaled, and the side-chain fragments from 0.01% to 1.57% are obtained, respectively. The abundance ratio of the products differs between the tests, but is similar for the anode and cathode sides in each test. Their total amount in the OCV-hold test is approximately four times as much as that in the load cycling test, corresponding to the FRR results, which indicates higher degradation rates in the OCV-hold test.

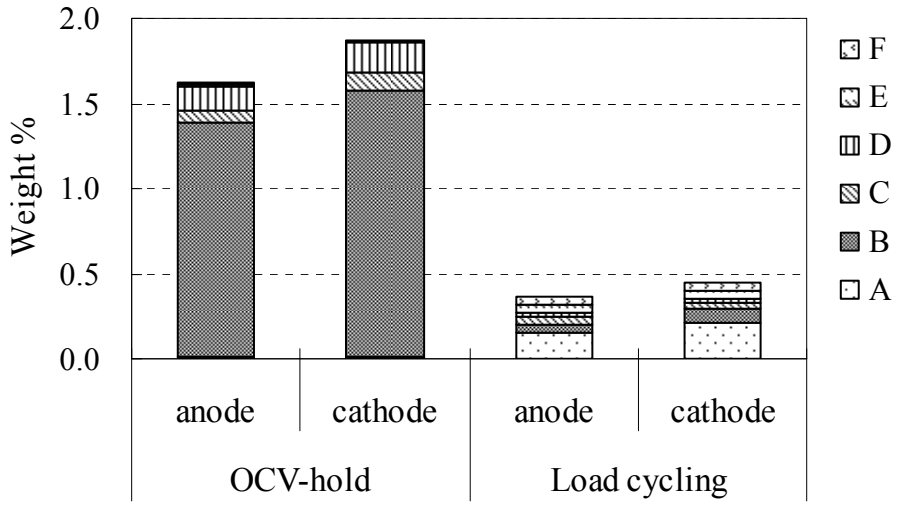

Figure 3-4. Abundance of the side-chain fragments in extracts of catalyst layers. See Table I for the chemical structures of A-F.

The signals from the PFSA polymer in ^{19}F NMR spectra for methanol extracts and the dissolved extraction residues were observed. The EW* and weight % of the PFSA polymer were quantitatively analyzed via ^{19}F NMR and are summarized in Figure 5. The weight %'s of PFSA polymer were calculated from the weight of PFSA polymer (using ^{19}F NMR) and the total weight of the catalyst layer (containing catalyst, carbon and PFSA polymer), which were measured before water extraction. The descriptions of EW*, the methanol extract and the dissolved extraction residue are described below. The findings considered in Figure 5 based on them are discussed.

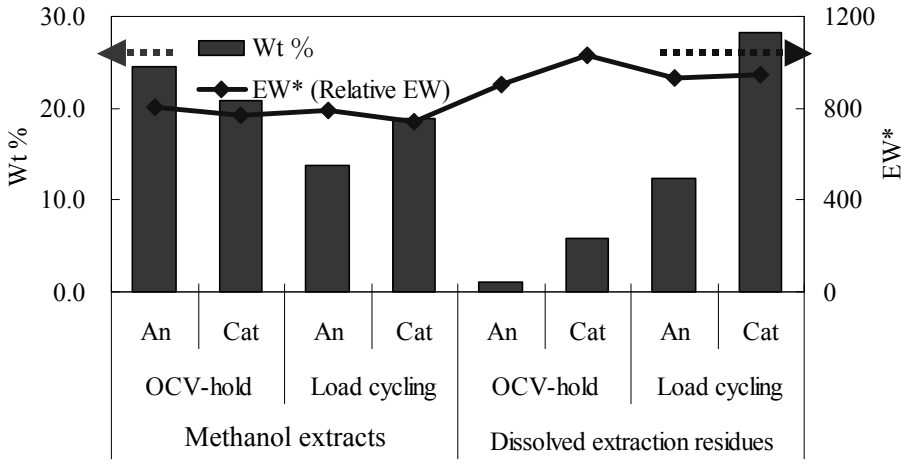

Figure 3-5. EW* values and amount of PFSA polymer in methanol extracts and dissolved extraction residues of catalyst layers. EW*all (average EW* of all PFSA polymer from wt % and EW* of methanol extracts and of dissolved extraction residues) were calculated, respectively, as follows: OCV-hold anode, 811; OCV-hold cathode, 827; load cycling anode, 858; and load cycling cathode, 865.

◆ EW is an important value which shows weight per one sulfo group in PFSA polymer. Therefore, it can also indicate the difference in chemical structure of the PFSA polymer. In this study, to investigate structural change in PFSA polymer in a catalyst layer, EW* was obtained. EW* has the same meaning as EW, and was calculated from the signal areas in ^{19}F NMR. In ^{19}F NMR of PFSA polymer in methanol or in a mixed solvent of water and propanol, the main-chain signal of PFSA polymer broadens, and the acquired area is slightly smaller than the actual area. For this reason, although EW* becomes smaller than EW (equivalent weight), it has a sufficient precision, and can be relatively compared between samples. For example, EW 1100 and EW 1000 actually show EW* 930 and EW* 860, respectively.

◆ Generally, the major portion of pristine PFSA polymer is not extracted into methanol, but dissolves into the mixed solvents of water and propanol only under high temperature and high pressure. PFSA polymer in methanol extracts has a low-molecular-weight or low EW* value. PFSA polymer in the dissolved extraction residues has approximately the usual molecular weight and EW*.

The change in PFSA polymer in the catalyst layers after the tests is evaluated as follows. While EW* of pristine PFSA is 930, EW* of the methanol extracts and

dissolved extraction residues (the two PFSA solutions) are 743-807 and 905-1034, respectively. EW*s of the methanol extracts are lower than those of the pristine PFSA, and EW*s of the dissolved extraction residues are almost equivalent to those of the pristine PFSA, or slightly higher. Then relative equivalent weight for all PFSA polymer (EW*all) in catalyst layer was calculated from EW*s and the weight %'s of PFSA polymer of the two kinds of PFSA solution. The values are shown in Figure 5, and the comparison between the tests is as follows.

EW*all: OCV-hold test < load cycling test

The reduction of EW*all means a reduced weight of moiety containing one sulfo group, and accordingly indicates main-chain scission of PFSA polymer. Furthermore, the remarkable reduction in the amount of PFSA polymer in the dissolved extraction residues after the OCV-hold test also suggests a reduction in molecular weight or main-chain scission.

3.3.2. Hydrogen peroxide vapor exposure tests

From the trap water analysis by ion chromatography and TOC measurement, weight loss of the membranes after HPV exposure tests can be decomposed into the generation of fluoride ion, TFA, other organics and other compounds (Figure 6). Under all humidity and temperature conditions used, the chemically stabilized membrane generates significantly less fluoride ion than the conventional membrane, proving the higher durability of stabilized membrane. However, decomposition products other than fluoride ion are generated. Moreover, under conditions of 30 %RH at 90 ºC and 100 ºC, the difference in weight loss between the two membranes was insignificant. Under conditions of 100 ºC, the stabilized membrane released more TFA and organic compounds into the trap water.

^{19}F NMR spectra of the extracts from the reference membranes and the membranes after HPV exposure tests (Figure 7) confirm the presence of one or two kinds of side-chain fragment. At 90 ºC, only fragment B in Table I is found for both stabilized and conventional membranes. At 100 ºC, another side-chain fragment D (Table I) is also found. These two fragments are quantitatively analyzed by ^{19}F NMR.

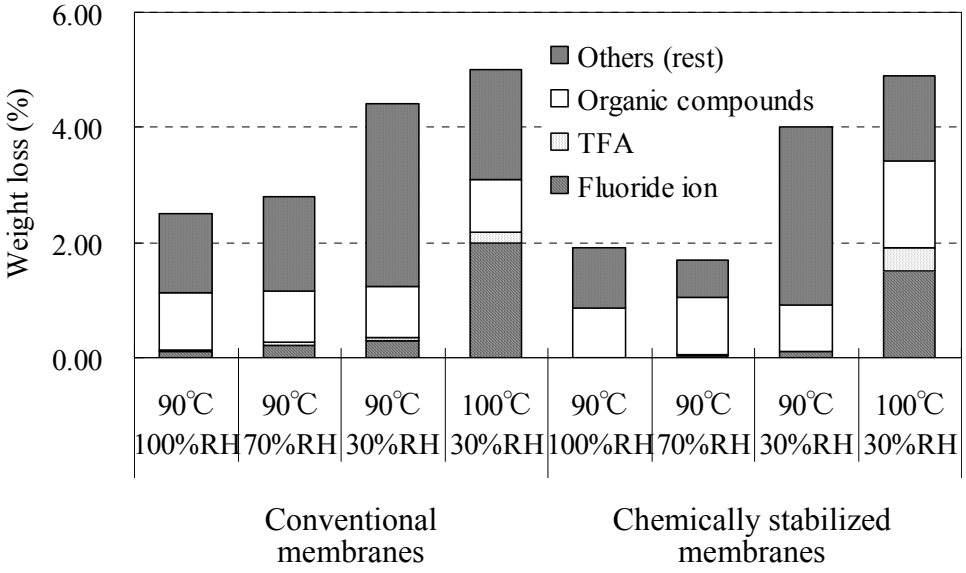

Figure 3-6. Weight loss analysis of PFSA membranes after HPV exposure tests.

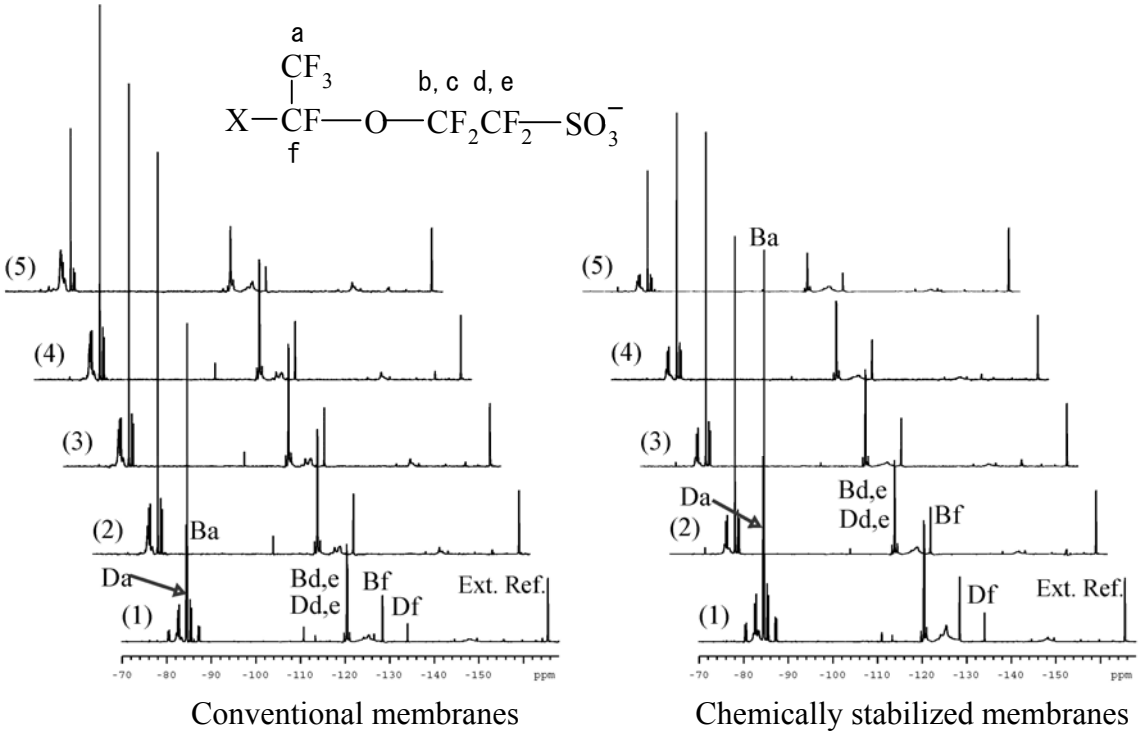

Figure 3-7. ^{19}F NMR spectra of the solvent extracts after HPV exposure tests. The conditions of temperature and relative humidity were as follows: (1) 100 ºC 30% RH; (2) 90 ºC 30% RH; (3) 90 ºC 70% RH; (4) 90 ºC 100% RH; and (5) reference (pristine membranes).

Figure 8 provides the weight % of the side-chain fragments generated during the tests. The weight % of the side-chain fragments in conventional membrane is lower than or almost equal to that in stabilized membrane at 90 ºC under all tested RH conditions. At 100 ºC, in contrast, the weight % of each fragment in the stabilized membrane exceeds that of the conventional membrane.

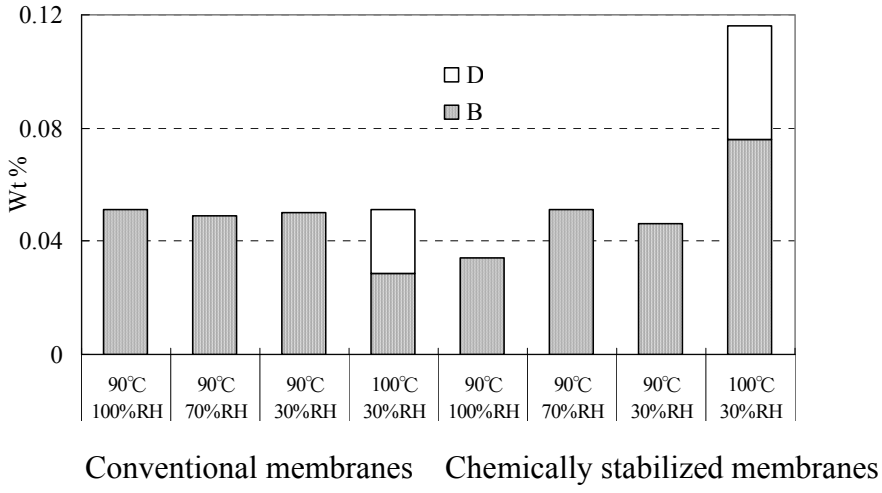

Figure 3-8. Weight of the side-chain fragments (B and D) in membranes generated during HPV tests. See Table I for the chemical structures of B and D.

Weight reduction of the membranes, TFA and TOC in trap water, and fragment weights in the membranes give a consistent result, wherein the stabilized membrane is not always more stable than the conventional membrane. This is in contrast to the evaluation based on FRR, which always implies the superior durability of the stabilized membrane under the conditions evaluated. We conclude that only FRR is not always a reliable indicator of PFSA polymer degradation. Organic compounds in trap water may contain the decomposition products generating from main-chain and side-chain scission. Decomposition products other than fluoride ion, probably containing main-chain and side-chain fragments, accounted for a significant portion of weight reduction of membranes due to degradation, their generation rates were not proportional to FRR. The generating rates of the other decomposition products should also be added to the reliable indicator of PFSA polymer degradation. The differences between the results of FRR measurement and decomposition product analysis strongly suggest the presence of two or more decomposition mechanisms in PFSA degradation.

3.4. Conclusions

1) The degradation PFSA polymer in the catalyst layers after an OCV-hold and a load cycling test were investigated by ^{19}F NMR.
   As degradation products, six kinds of the side-chain fragments were acquired from the water extracts and the methanol extracts, the weight of each of which was from 0.01 wt% to 1.57 wt % of the catalyst layers. The side-chain fragments indicate that side-chain scission occurs. Two kinds of them are obtained from the membranes after HPV exposure tests described later. Moreover, reduction of EW*all and amounts of PFSA polymer in catalyst layer after the tests suggests that main-chain scission occurs.
2) PFSA polymer degradation after an HPV exposure test was investigated using ion chromatography and TOC for trap water, and using ^{19}F NMR for water/methanol extracts of membranes. As degradation products, fluoride ion, TFA, other organics and other compounds are acquired from trap water, and two kinds of side-chain fragments are acquired from water/methanol extracts of membranes, respectively, and they were quantified.
3) Decomposition products other than fluoride ion accounted for a significant portion of membrane weight loss due to degradation. Moreover, the generation rates of the weight loss, TFA and TOC in trap water, and fragment weights in the membranes were not always proportional to FRR. We conclude that generation rate of the other decomposition product is also reliable indicator of PFSA polymer degradation, as well as FRR, to ensure more precise evaluation of PFSA polymer degradation.

3.5. Acknowledgements

This work was partially supported by a grant from Research and Development of Polymer Electrolyte Fuel Cells from New Energy and Industrial Technology Development Organization (NEDO), Japan.

3.6. References of chapter 3

1. D. E. Curtin, R. D. Lousenberg, T. J. Henry, P. C. Tangeman, and M. E. Tisack, *J. Power Sources* **2004**, *131*, 41.
2. E. N. Balko and J. T. Chaklos, *J. Appl. Polym. Sci.* **1981**, *26*, 1519.

3. A. Pozio, R. F. Silva, M. De Francesco and L.Giorgi, *Electrochim. Acta* **2003**, *48*, 1543.
4. M. Aoki, H. Uchida and M. Watanabe, *Electrochem. Commun.* **2005**, 7, 1434.
5. V. O. Mittal, H. R. Kunz and J. M. Fenton, *Electrochem. Solid-State Lett.* **2006** *9*, A299.
6. V. O. Mittal, H. R. Kunz and J. M. Fenton, *J. Electrochem. Soc.* **2006***, 153*, A1755.
7. T. Kinumoto, M. Inaba, Y. Nakayama, K. Ogata, R. Umebayashi, A. Tasaka, Y. Iriyama, T. Abe and Z. Ogumi, *J. Power Sources* **2006***, 158*, 1222.
8. W. Liu, K. Ruth and G. Rusch, *J. New Mater. Electrochem. Syst.* **2001**, *4*, 227 .
9. M. Aoki, H. Uchida and M. Watanabe, *Electrochem. Commun.* **2006**, *8*, 1509 .
10. J. Healy, C. Hayden, T. Xie, R. Waldo, M. Brundage, H. Gasteiger, and J. Abbott, *Fuel Cells* **2005**, ***5***, 302.
11. M. Takasaki, N. Sato, K Ookubo, K. Goto, K. Kimura, Y. Sakiyama, G. Katagiri, T. Minamide, H. Nakayama, and M. Hori, *Polymer Preprints, Japan* **2007**, *56*, 4509.
12. N. Sato, K Ookubo, E. Hayashi, M. Takasaki, Y. Sakiyama, G. Katagiri, T. Minamide, H. Nakayama, and M. Hori, *2007 Fuel Cell Seminar preprints*.
13. T. Kinumoto, M. Inaba, Y. Nakayama, K. Ogata, R. Umebayashi, A. Tasaka, Y. Iriyama, T. Abe and Z. Ogumi, *J. Power Sources* **2006**, *158*, 1222.
14. H. L. Tang, P. K. Shen, S. P. Jiang, W. Fang and P. Mu, *J. Power Sources* **2007**, *170*, 85.
15. A. Collier, H. J. Wang, X. Z. Yuan, J. J. Zhang and D. P. Wilkinson, *Int. J. Hydrogen Energy* **2006**, *31*, 1838.
16. F. M. Collette, C. Lorentz, G. Gebel and F. Thominette, *J. Membr. Sci.* **2009**, *330*, 21.
17. C. Zhou, M. A. Guerra, Z. M. Qiu, T. A. Zawodzinski and D. A. Schiraldi, *Macromolecules* **2007**, *40*, 8695.
18. L. Ghassemzadeh, M. Marrony, R. Barrera, K. D. Kreuer, J. Maier and K. Mu¨ller, *J. Power Sources* **2009**, *186*, 334.
19. L. Ghassemzadeh, K.-D. Kreuer, J. Maier, and K. C. Müller, *J. Phys. Chem.* **2010**, *114*, 14635.
20. R. Hommura, K. Kawahara, and T. Shimodaira, *Polymer Preprints Japan* **2005**, *54*, 4517.
21. K. Hatada, Y. Terawaki, T. Kitayama, *Kobunshi Ronbunshu* **1992**, ***49***, 335.

22. M. Takasaki, K. Kimura, K. Kawaguchi, A. Abe, G. Katagiri, *Macromolecules* **2005**, *38*, 6031.
23. Q. Chen, K. Schmidt-Rohr, *Macromolecules* **2004**, *37*, 5995.

Chapter 4 Complete NMR Assignment of a Sulfonated Aromatic Block Copolymer via Heteronuclear Single-Quantum Correlation, Heteronuclear Multiple-Bond Correlation and Heteronuclear Single-Quantum Correlation Total Correlation Spectroscopy

4.1. Introduction to Chapter 4

Proton exchange membrane fuel cells (PEMFCs) are expected to be used as alternative power sources, especially for applications in electric vehicles and residential units. Proton exchange membranes (PEMs) are an essential component of PEMFCs. Although perfluorinated sulfonic acid polymers, such as Nafion^{TM}, are most often used as PEMs, nonfluorinated aromatic ionomers have been extensively investigated. Sulfonated aromatic block copolymers (SABCs) are one of nonfluorinated PEM materials, and their excellent physical properties have been reported.[1-5] To further improve the properties of SABCs, it is crucial to understand how their physical properties depend upon their chemical structure. In addition, for practical applications, the degradation mechanisms during PEMFC operation, resulting in changes of the chemical structure, should be investigated in detail. A necessary first step is to determine the precise chemical structures of pristine membranes. Because NMR is a powerful tool for determining the chemical structures of polymers, it is possible to elucidate the chemical structures of pristine and posttest membranes. The complex structure of SABCs makes the NMR analysis difficult: for example, the present case contains five different phenylene rings. Here we report a successful NMR assignment of pristine SABC based on heteronuclear single-quantum correlation (HSQC),[6, 7, 8, 9] heteronuclear multiple-bond correlation (HMBC)[10, 11, 12] and heteronuclear single-quantum correlation total correlation spectroscopy (HSQC-TOCSY)[13, 14] techniques.

4.2. Experimental procedures

4.2.1. Materials

The chemical structure, number average molecular weight (Mn), molecular weight distribution (Mw/Mn), copolymer composition (w/z), and calculated ion exchange capacity (IEC) of the SABC are shown in Figure 1. The SABC consists of hydrophobic and hydrophilic blocks. The hydrophilic blocks contain a substructure of sulfonated

fluorenylidene biphenylene. The SABC was synthesized with F-terminated telechelic oligomers[1] (DP (degree of polymerization) =21) and OH-terminated telechelic oligomers[1] (DP=8). The IEC of the SABC was measured by titration after the ion exchange, resulting in a value of 1.78 meq.g^{-1}.

We used F-terminated telechelic oligomer as the model oligomer for the NMR assignment of the SABC. The chemical structure of the model oligomer is also shown in Figure 1.

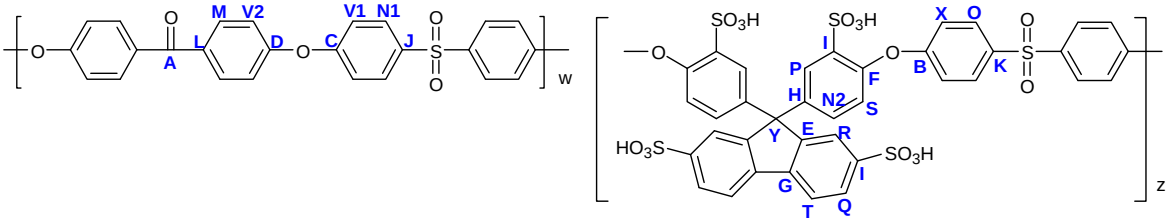

SABC (Mn=116,000*1, Mw/Mn=2.01*1, w/z=72/28*2, IEC=2.00*2
*1 Actual value, *2 Theoretical value)

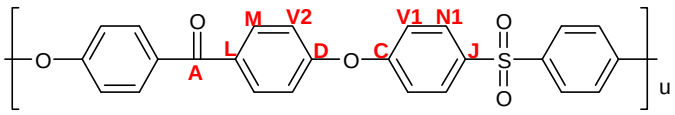

The model oligomer

Figure 4-1. Chemical structures of SABC and the model oligomer.

4.2.2. NMR experiments

All NMR spectra were acquired with a Varian UNITY INOVA 500 in deuterated dimethyl sulfoxide (using tetramethylsilane as the internal reference) at frequencies of 499.8 MHz and 125.7 MHz for ^{1}H and ^{13}C NMR, respectively. The concentration of the sample solutions was 50 mg in 0.6 mL. ^{1}H NMR experiments were conducted at 25, 50, 70, 90 and 110°C. All NMR experiments were executed at 60°C. In the HSQC, HMBC and HSQC-TOCSY experiments, which were all gradient-selected experiments, a total

of 256, 400 and 256 spectra, each containing 2048 data points, were accumulated, respectively.

4.3. Results and discussion

4.3.1. ^{1}H NMR spectrum of the SABC and the temperature effect

Figure 2a shows the ^{1}H NMR spectrum for the SABC at 25°C. The lower-case letter labels in Figure 2 represent ^{1}H signals (the detail is described later). Because of the complex structure, with five different phenylene rings, 12 types of ^{1}H signals were observed in the narrow chemical shift range between 7.0 and 8.0 ppm. Because these ^{1}H signals are overlapping or close, a precise NMR assignment was not possible with such insufficient ^{1}H signal separation. Therefore, the following two strategies were executed to separate the signals:

1) The solvent and the temperature effect for ^{1}H NMR experiments were examined. By optimizing the solvent and temperature conditions, the signals were sharpened and separated.

2) The ^{1}H and ^{13}C signals of the hydrophobic blocks were assigned in advance using the model oligomer, and then those of the hydrophilic blocks were assigned. Thus, the signals of the hydrophobic and hydrophilic blocks were separated.

First, the solubility of the SABC in other solvents (pyridine, 1,1,1,3,3,3-hexafluoroisopropanol and methanol) was examined. However, the SABC was insoluble in any of these solvents. Next, the effect of temperature on the ^{1}H NMR experiments was examined. Figures 2b, 2c, 2d and 2e show the ^{1}H NMR spectra of SABC at 50, 70, 90 and 110°C, respectively. In general, signals become sharper at higher temperatures. The separation of the signals within the temperature range is as follows:

The signal ‘q’ was separated from ‘m’ and ‘o’ at 25, 50 and 70°C, and the signal separation was better at lower temperatures. The signals ‘s’, ‘x’, ‘n2’, ‘v1’ and ‘v2’ were separated from other signals above 50°C, and the separations were better at higher temperatures. Accordingly, 50 and 70°C were the most suitable for the ^{1}H NMR experiment. It was determined that all the NMR experiments, which took more than five days, would be conducted at 60°C so that the chemical structure of the SABC would not change during the experiments.

4.3.2. NMR assignment for the SABC

Figure 3 shows the ^{1}H NMR (top), ^{13}C NMR (middle) and HSQC (bottom)[6-9] spectra of the SABC at 60°C.

In the ^{1}H NMR spectrum at 60°C, the lower-case letter labels from 'm' to 'x' (except for 'u' and 'w') are attached to all ^{1}H signals, and they represent the ^{1}H signals (described in detail later).

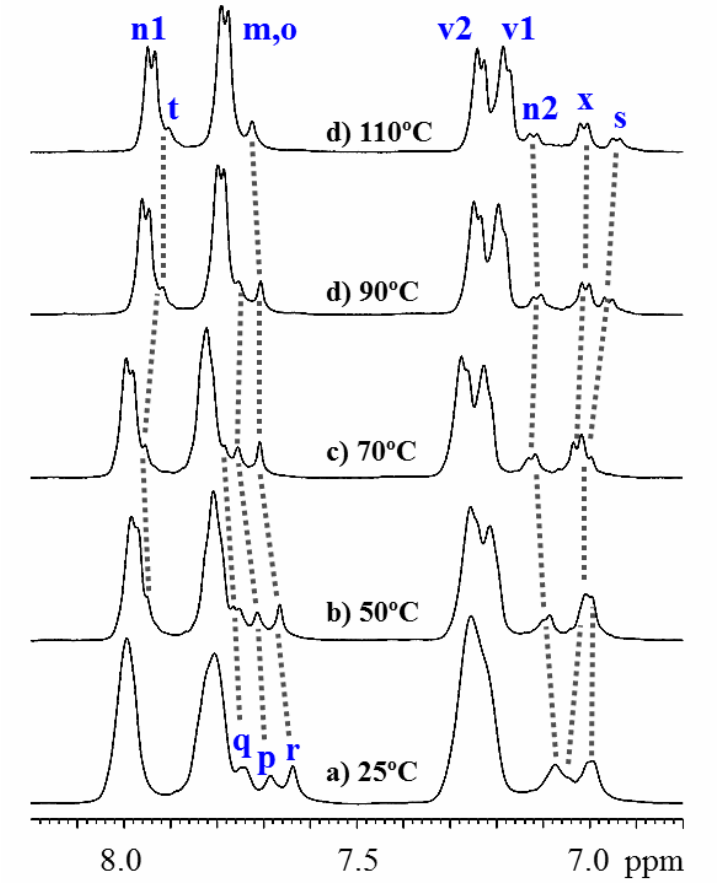

Figure 4-2. ^{1}H NMR spectra of SABC at a) 25°C; b) 50°C; c) 70°C; d) 90°C and e) 110 °C. The small letters attached to the ^{1}H signals (from 'm' to 'x') correspond to the capital letters (from 'M' to 'X') shown in the chemical structure of SABC (Figure 1).

In the ^{13}C NMR spectrum, 24 different types of signals arising from 5 different phenylene rings are observed from 117.8 to 161.6 ppm. The upper-case letter labels from 'A' to 'Y' (except for 'U' and 'W') are attached to the ^{13}C signals from 192.5 to 64.4 ppm, in order. The upper-case letter labels represent the ^{13}C signals. The chemical shifts of many ^{13}C signals are close. 'N1' and 'N2' completely overlap, and 'V1' and 'V2' almost overlap in the ^{13}C NMR spectrum. The two pairs of signals are separated in HSQC and HMBC (shown later). Therefore, they are indicated as 'N1', 'N2', 'V1' and 'V2'. 'I', which will later be assigned to two ^{13}C signals, is not separated into the two ^{13}C signals in HMBC and does not have an HSQC correlation (shown later). Therefore, 'I' is not indicated by 'I1' and 'I2'.

The HSQC spectrum gives correlations between ^{1}H and ^{13}C nuclei that are one bond apart. All 12 HSQC correlations are observed in Figure 3. The lower-case letter labels are attached to the ^{1}H signals, corresponding to the upper-case letter labels of the ^{13}C signals with which the ^{1}H signals correlates in the HSQC spectrum, respectively. The HSQC spectrum indicates that the signals of 'x' and 's' still overlap, and other ^{1}H signals are observed to be very close together. The correlations of 'x-X' and 's-S' were identified by the intensity of the correlations with 'X' and 'S'.

The following analysis for the hydrophobic blocks was performed using the model oligomer, based on the HMBC technique.

4.3.3. The hydrophobic blocks

Table 1 gives the chemical shift assignments of the model oligomer. These data were obtained based on the results of ^{1}H NMR, ^{13}C NMR, HSQC, correlation spectroscopy (COSY) and HMBC of the model oligomer, which are shown in Figures SI4-1, SI4-2, SI4-3, SI4-4 and SI4-5. The correspondence of the signals of the model oligomer to SABC was presumed and is shown in Table 1. The chemical shift assignment of the hydrophobic blocks was confirmed, mainly by HMBC, as follows. The HMBC spectra of SABC are shown in Figure 4. The HMBC spectrum yields correlations between ^{1}H and ^{13}C nuclei that are two or three bonds apart. All the ^{1}H and ^{13}C signals from the hydrophobic blocks were confirmed by Table 1. ^{1}H and ^{13}C chemical shift assignments of SABC and the model oligomer correlations with the ^{1}H signals of 'v1', 'v2', 'm' and 'n1' acquired from the HMBC spectra. Thus, the ^{1}H and ^{13}C signals of the hydrophobic blocks were assigned.

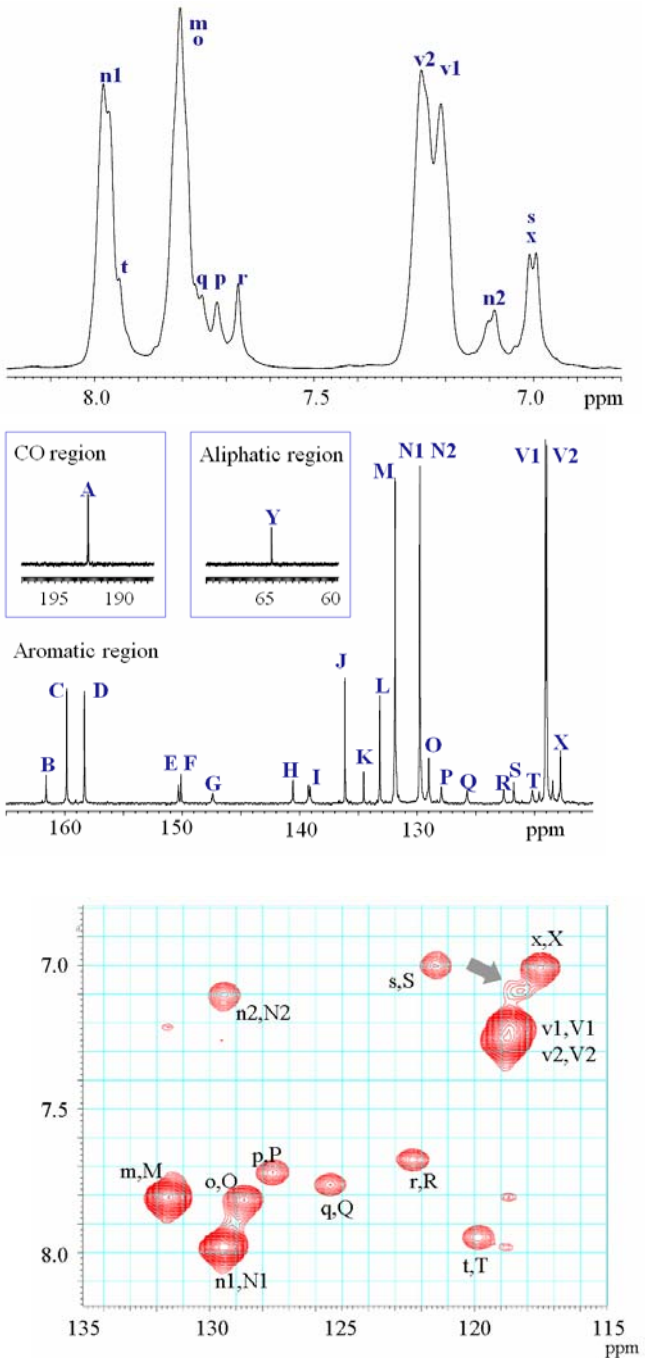

Figure 4-3. ^{1}H NMR (top), ^{13}C NMR (middle) and HSQC (bottom) spectra of SABC at 60 °C. In HSQC, the vertical axis represents the ^{1}H chemical shift, and the horizontal axis represents the ^{13}C chemical shift. $^{1}J_{CH}$=140 Hz was used.

Table 4-1. ^{1}H and ^{13}C chemical shift assignments for the SABC and the model oligomer.

SABC				the model oligomer			
^{13}C chemical shift (ppm)		^{1}H chemical shift (ppm)*1		^{13}C chemical shift (ppm)		^{1}H chemical shift (ppm)	
A	192.5	-	-	A	193.8	-	-
B	161.6	-	-	-	-	-	-
C	159.8	-	-	C	160.5	-	-
D	158.3	-	-	D	159.0	-	-
E	150.3	-	-	-	-	-	-
F	150.1	-	-	-	-	-	-
G	147.4	-	-	-	-	-	-
H	140.6	-	-	-	-	-	-
I	139.2 139.1	-	-	-	-	-	-
J	136.1	-	-	J	136.6	-	-
K	134.5	-	-	-	-	-	-
L	133.2	-	-	L	133.7	-	-
M	131.9	m	7.81	M	132.4	m	7.85
N1	129.8	n1	7.98	N1	130.0	n1	7.95
N2		n2	7.10	-	-	-	-
O	129.0	o	7.82	-	-	-	-
P	127.9	p	7.72	-	-	-	-
Q	125.7	q	7.78	-	-	-	-
R	122.6	r	7.68	-	-	-	-
S	121.8	s	7.00	-	-	-	-
T	120.2	t	7.94	-	-	-	-
V1	119.1	v1	7.24	V1	119.1	v1	7.15
V2	119.0	v2		V2		v2	7.12
X	117.8	x	7.01	-	-	-	-
Y	64.4	-	-	-	-	-	-

*1 The chemical shifts of the SABC were obtained from HSQC spectrum.

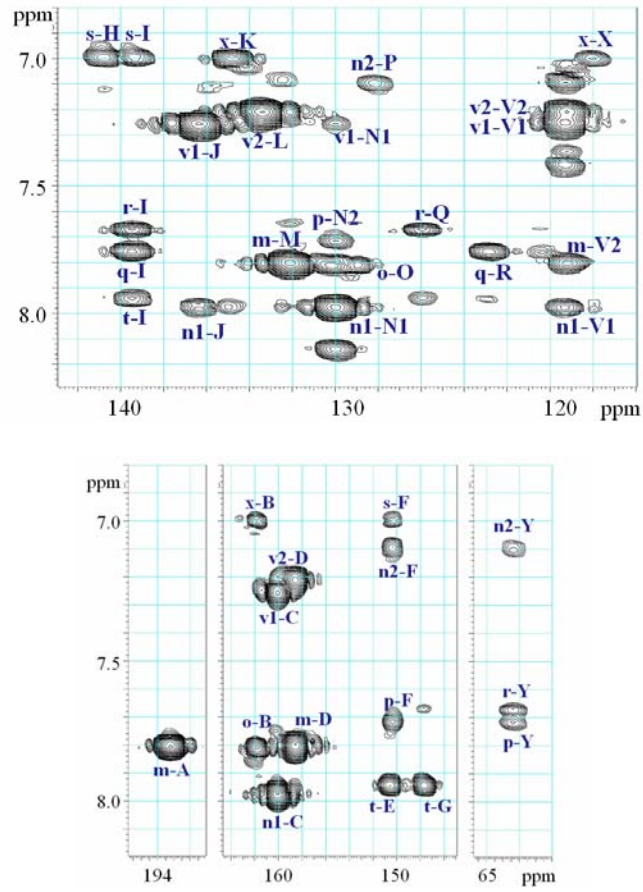

Figure 4-4. HMBC spectra of SABC at 60 °C. The vertical axis represents the ^{1}H chemical shift, and the horizontal axis represents the ^{13}C chemical shift. $^{1}J_{CH}$=140 Hz, $^{n}J_{CH}$=8 Hz were used.

4.3.4. The hydrophilic blocks

We then tried to assign the hydrophilic blocks of the SABC in the same way as for the hydrophobic blocks. However, we were not successful for the following two reasons:

1) Some HMBC correlations of n2-S, q-T, r-E, r-G, q-G, n2-H, p-H and o-X are not acquired. The reason was assumed to be that $^{n}J_{CH}$ (8 Hz) was not appropriate for all of the ^{1}H and ^{13}C signals of the SABC.

2) As some of HMBC correlations were not identified for the overlapping between ‘x’ and ‘s’, ‘x’ and ‘s’ could not be assigned.

Then, we applied HSQC-TOCSY, in which the correlations are observed without any relation to $^{n}J_{CH}$. It was expected that all HSQC-TOCSY correlations would be acquired and that HSQC-TOCSY would lead to the assignments of ‘x’ and ‘s’.

Figure 5 shows the HSQC-TOCSY spectrum of the SABC. In the HSQC-TOCSY spectrum, correlation signals among all ^{1}H signals having spin-spin coupling (TOCSY correlations) and HSQC correlations are acquired. All HSQC-TOCSY correlations of the hydrophilic blocks were acquired with good separation and were identified as follows: r-Q, q-Q, t-Q, r-R, q-R, t-R, r-T, q-T, t-T, n2-P, p-P, (s-P), n2-S, p-S, s-S, n2-N2, p-N2, (s-N2), o-X, x-X, o-O and (x-O). The correlations shown in parentheses, (s-P), (s-N2) and (x-O), were not identified by the correlations alone because of the overlapping between ‘s’ and ‘x’. However, they can be identified by other correlations of p-S, n2-S and o-X. Based on the HSQC-TOCSY correlations, the following three groups of proton signals of [r, q, t], [n2, p, s] and [o, x] were determined to exist on the same phenylene rings, respectively. Moreover, ‘p’, ‘s’ and ‘n2’ were assigned based on the HMBC correlations for n2-P, n2-Y and p-Y, and ‘r’, ‘q’ and ‘t’ were assigned based on the HMBC correlations for q-R and r-Y. Consequently, the HMBC correlations from ‘s’ and ‘x’ of s-F, s-H, s-I, x-B, x-K and x-X were identified, and they led to the assignment of ‘s’ and ‘x’. Thus, all ^{1}H and ^{13}C signals were assigned by other HMBC correlations without inconsistency. The results are summarized in Table 1.

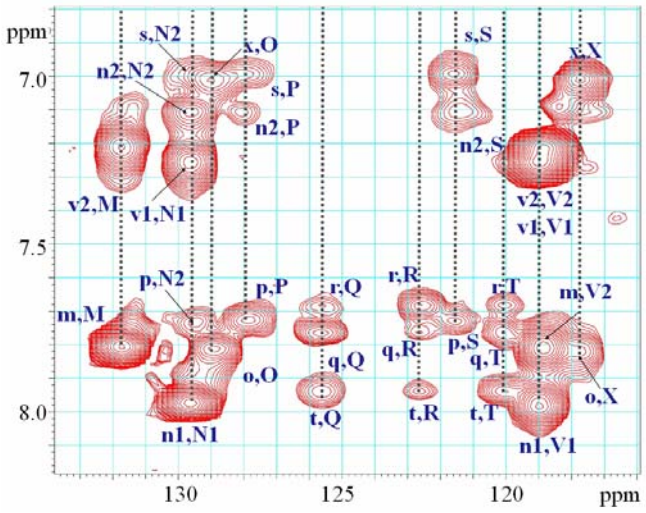

Figure 4-5. HSQC-TOCSY spectrum of SABC at 60 °C. The vertical axis represents the ^{1}H chemical shift, and the horizontal axis represents the ^{13}C chemical shift. A mixing time 100 ms was used.

As described above, the complete NMR assignment of the SABC was performed, and it was supported by the following two facts:
1) In Figure 2d and Figure 2e, ‘n2’, ‘x’, and ‘s’ indicate doublet splitting and the ^{1}H signal strengths.
2) In Figure 2b, ‘q’ indicates doublet splitting.

Generally, in NMR spectra of block copolymers, NMR signals based on the junction points for each block are observed separately. However, in the NMR spectra of the SABC under the experimental conditions in this study, the signals of the junction points for each block were not separated from each other for the following reason. In both the hydrophobic blocks and the hydrophilic blocks of the SABC, the 1,4-phenylene ether-sulfone (ES) unit is present. That is, two types of ES units neighboring the 1,4-phenylene ether-ketone unit and neighboring sulfonated fluorenylidene biphenylene exist, and they have already been assigned. Thus, the ^{1}H and ^{13}C NMR signals of the ES unit separated based on diad
sequence and did not separate based on triad-or-higher sequences. The NMR signals of junction points for each block arise when the NMR signals of the ES unit are separated on the basis of triad-or-higher sequences.

4.3.5. Copolymer composition and IEC

The IEC and copolymer composition (*w*/*z* mol%) were calculated based on the integrated intensities of some ^{1}H signal areas. Table 2 gives the integrated intensities of some ^{1}H signal areas and the calculating formula. The copolymer composition of *w*/*z*=76/24 (mol%) was calculated. The IEC obtained by NMR was 1.81 meq/g, which was in good agreement with that obtained by titration (1.78 meq.g^{-1}). Consequently, the validity of the NMR assignment was supported.

As mentioned above, the theoretical composition ratio is *w*/*z*=72/28 (mol%). In contrast, *w*/*z*=76/24 (mol%) was obtained from the NMR results. The composition ratio of *z* (mol%) obtained from NMR was smaller than the theoretical one. It was assumed that the difference in the two values was based on the following reasoning:
The SABC was synthesized by sulfonation after copolymerization of the two telechelic oligomers. The theoretical composition ratio (*w*/*z*) is 72/28 when all the fluorenylidene biphenylene substructures are substituted by four sulfo groups. Sulfonated fluorenylidene biphenylene substructures with three or fewer sulfo groups existed, and the NMR signals were broadened or were not observed all. That is because the

sulfonated substructures with three or fewer sulfo groups do not dissolve easily in DMSO. The HSQC signal indicated by an arrow in Figure 3 was presumed to be assigned to one of the less sulfonated substructures.

Table 4-2. The integrated intensities of the ^{1}H signals and the formula for calculating the copolymer composition and the IEC

The integrated intensities of the ^{1}H signals	
I (v1, v2)[a]	310.57
I (s, x, n2)[b]	100.00
The calculating formula	
w (mol %):	
I(v1, n1, v2, m) ×100 / {I(s, x, n2) + I(v1, n1, v2, m)}	
= 310.57 / (100.00+310.57)	
z (mol %):	
I(s, x, n2) ×100 / {I(s, x, n2) + I(v1, n1, v2,m)}	
= 100.00 / (100.00+310.57)	
IEC (eq.g^{-1}):	
$\frac{z \text{ mol\%} \times 4}{(w \text{ mol\%} \times \text{m.w. HPO}^{c} + z \text{ mol\%} \times \text{m.w. HPI}^{d})}$	

[a]Integrated intensities of 'v1' and 'v2' signals.
[b]Integrated intensities of 's', 'x' and 'n2' signals.
[c]m.w. of the hydrophobic blocks ($C_{25}H_{16}O_5S$): 428.46.
[d]m.w. of the hydrophilic blocks ($C_{37}H_{24}O_{16}S_5$): 884.90.

4.3.6. Post-test analyses of the SABC membrane

The ^{1}H and ^{13}C NMR assignments of SABC were successfully and perfectly performed as above-mentioned. Using the assignments, the structural analysis of the post-test membrane was conducted.[15] According to the literature, following changes of

the post-test membrane in ^{1}H and ^{13}C NMR spectra were reported. 1) The ^{1}H NMR spectrum was broader for the post-test membrane. 2) In the ^{13}C NMR spectrum of post-test membrane, the intensity of I signal (carbon which combined to sulfo group) decreased. 3) G signal (one of the fluorenyl carbons) shifted to lower magnetic field. Therefore it was reported that the NMR data suggest structural changes in the sulfonic acid-containing fluorenyl groups.

Therefore, the important data for elucidating a degraded structure of SABC were given by this study.

4.4. Conclusions

Complete NMR assignment of the SABC was performed using HSQC, HMBC and HSQC-TOCSY. Owing to the complex structure of the SABC with sequenced hydrophilic and hydrophobic blocks, the ^{1}H NMR spectrum of the SABC at 25°C demonstrates insufficient separation of ^{1}H signals. The signal separation was improved by optimizing the temperature conditions for the ^{1}H NMR experiment, and all NMR experiments were conducted at 60°C. The ^{1}H and ^{13}C NMR chemical shift assignments of the hydrophobic blocks were executed based on HSQC and HMBC with reference to those of a model oligomer. For the ^{1}H and ^{13}C NMR chemical shift assignments of the hydrophilic blocks, HMBC correlations that were necessary and sufficient for the complete assignment were not acquired, and some HMBC correlations were not identified. Then, HSQC-TOCSY was applied. All HSQC-TOCSY correlations were obtained, and HSQC-TOCSY identified the unidentified HMBC correlations. Thus, all of the ^{1}H and ^{13}C signals of the hydrophilic blocks were successfully assigned. The copolymer composition (w/z=76/24 mol%) and the IEC (1.81 meq/g) for the SABC were obtained based on the chemical shift assignment and the integrated intensities of some ^{1}H NMR signals. The IEC value obtained from the ^{1}H NMR spectra was consistent with that obtained via titration (1.78 meq/g). Then degradation analysis of SABC was conducted using assignments of the ^{1}H and ^{13}C NMR signals which were obtained in this research, and the degraded structure of SABC was shown.[15] Therefore, the important data for elucidating a degraded structure of SABC were given by this study.

The authors performed a complete NMR assignment of an SABC. This approach is applicable to other emerging aromatic polymer with complex structures and the posttest

membrane. The application to posttest membranes elucidates the changes in the chemical structure and the degradation mechanism of the polymer membranes, which will further promote the development of high-performance PEM materials.

4.5. Acknowledgements

This work was partly supported by the New Energy and Industrial Technology Development Organization (NEDO) of Japan through funds for the "Research on Nanotechnology for High-Performance Fuel Cells" ("HiPer-FC") project.

4.6. Supplementary Information accompanies the paper;

^{1}H NMR, ^{13}C NMR, HSQC, COSY, HMBC spectra of the model oligomer in $CDCl_3$.

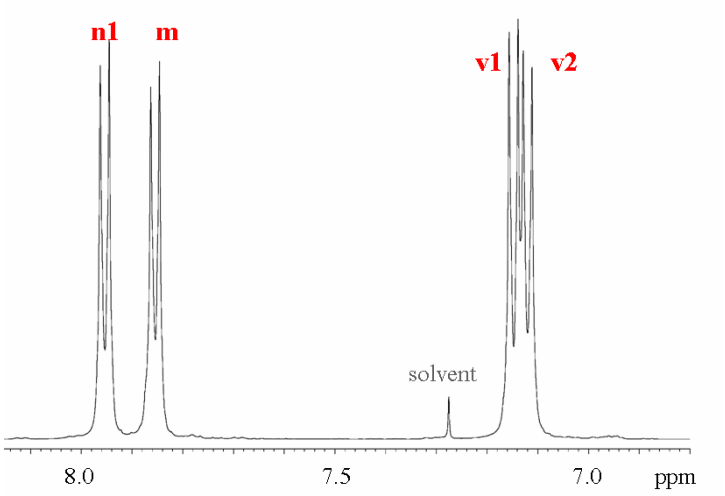

Figure SI4-1. ^{1}H NMR spectrum of the model oligomer in $CDCl_3$.

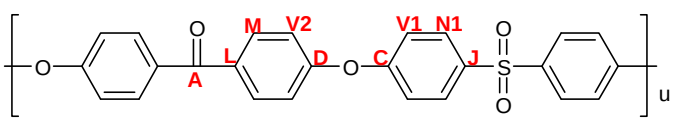

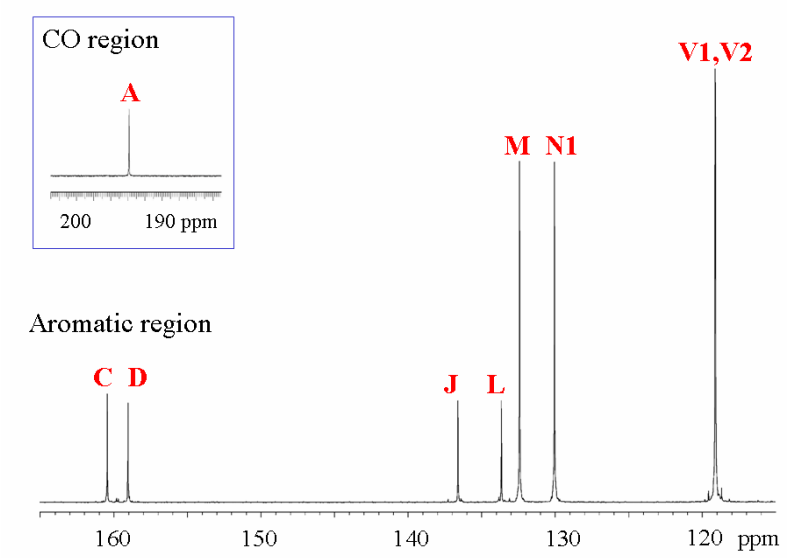

Figure SI4-2.^{13}C NMR spectrum of the model oligomer in $CDCl_3$.

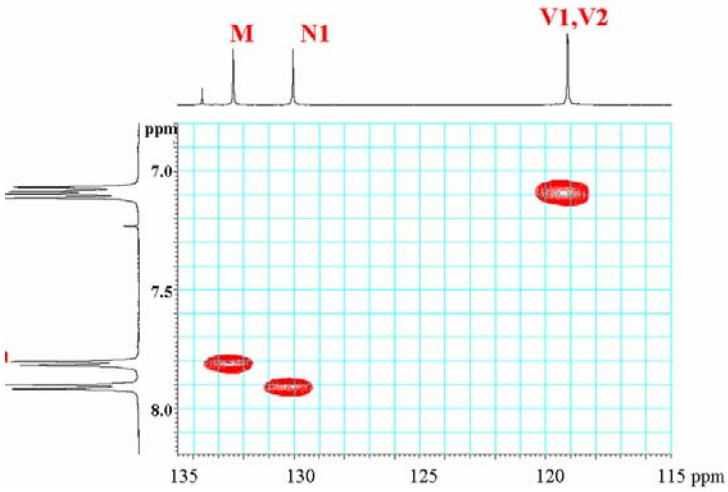

Figure SI4-3. HSQC spectrum of the model oligomer.

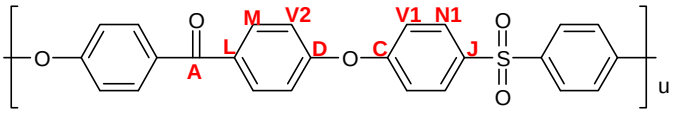

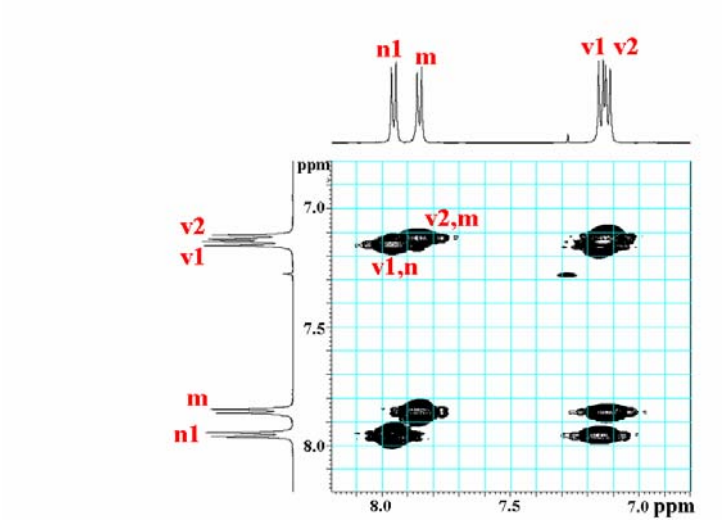

Figure SI4-4. COSY spectrum of the model oligomer.

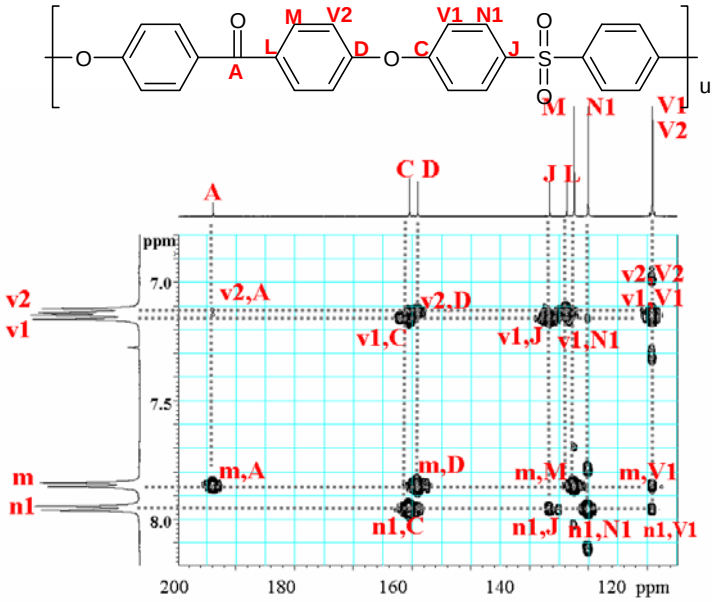

Figure SI4-5. HMBC spectrum of the model oligomer.

4.7. References of chapter 4

1. Bae, B., Miyatake, K., Watanabe, M., *Macromolecules* **2010,** *43*, 2684.
2. Bae, B., Miyatake, K., Watanabe, M., Macromolecules **2009**, *42*, 1873.
3. Bae, B., Miyatake, K., Watanabe, M., *ACS Appl. Mater. Interfaces* **2009**, *1*, 1279.
4. Chikashige, Y., Chikyu, Y., Miyatake, K., Watanabe, M., *Macromolecules* **2005**, *38*, 7121.
5. Tanaka, M., Koike, M., Miyatake, K., Watanabe, M., *Macromolecules* **2010**, *43*, 2657.
6. Palmer III, G. A., Cavanagh, J., Wright, E. P., Rance, M., *J. Magn. Reson*. **1991**, *93*, 151.
7. Kay, E. L., Kelfer, P., Saarinen, T., *J. Am. Chem. Soc*. **l992**, *114*, 10663.
8. Kontaxis, G., Stonehouse, J., Laue, D. E., Keeler, *J. Magn. Reson. Ser. A* **1994**, *111*, 70.
9. Sehleucher, J., Schwendinger, M., Sattler, M., Schmidt, P., Schedletzky, O., Glaser, J. S., Sørensen W. O., Griesinger C., *J. Biomol. NMR* **1994**, *4*, 301.
10. Bax, A., Summers, F. M., *J. Am. Chem. Soc*. **1986**, *108*, 2093.
11. Willker, W., Leibfritz, D., Kerssebaum, R., Bermel, W., *Magn. Reson. Chem*. **1993**, *31*, 287.
12. Ruiz-Cabello, J., Vuister, W. G., Moonen, W. T. C. van Gelderen, P., Cohen, S. J., van Zijl, M. C. P., *J. Magn. Reson*. **1992**, *100*, 282.
13. Kövér, E. K., Prakash, O., Hruby, J. V., *J. Magn. Reson. Ser. A* **1993**, *103*, 92.
14. Kövér, E. K., Hruby, J. V., Uhrín, D., *J. Magn. Reson*. **1997**, *129*, 125.
15. Byungchan Bae, Kenji Miyatake, Makoto Uchida, Hiroyuki Uchida, Yoko Sakiyama, Takeou Okanishi, Masahiro Watanabe, *ACS Appl. Mater. Interfaces* **2011**, *3*, 2786.

Chapter 5 Conclusions of this study

In this study, the chemical structures of pristine polymer electrolytes (a PFSA electrolyte, Nafion and a hydrocarbon electrolyte, SABC) and those of the degradation products of PFSA electrolyte after PEMFC operation and hydrogen peroxide vapor (HPV) exposure tests were primarily investigated by NMR.

The contents of each chapter are summarized below.

5.1. Conclusions of chapter 2

We demonstrate ^{19}F and ^{13}C NMR assignments and study of the structure in solution of Nafion, a perfluorosulfonate ionomer. Using ^{19}F–^{13}C HSQC, ^{19}F–^{13}C CIGAR–HMBC, and ^{19}F–^{19}F COSY to the model compounds of Nafion, we determine ^{19}F and ^{13}C assignments of model compounds. The combination of the three 2D NMR experiments represents an entirely new approach to analysis of perfluorinated organic compounds. On the basis of the assignments of the model compounds and also based on ^{19}F coupled and ^{19}F complete decoupled ^{13}C NMR for Nafion, ^{19}F and ^{13}C NMR assignments are determined for Nafion. In this study the two ^{13}C signals (OCF_2) in the side chain separate more clearly relative to previously reported results. We also carried out MALDI–MS for Nafion, supporting the results found in NMR. From the result of NMR, it is suggested that the aggregates of Nafion in solution exist, and the structure of the aggregates is estimated.

5.2. Conclusions of chapter 3

Operation tests were applied to fuel cell with perfluorosulfonic acid (PFSA) polymer for membranes and electrodes. Degradation of PFSA polymer in catalyst layers after the tests was investigated using ^{19}F NMR. As the decomposition products, six kinds of the side-chain fragments were acquired from the water and the methanol extracts, and the each weight of the fragment was acquired. The side-chain fragments indicate that side-chain scission occurs at two positions in the side-chain. Moreover, reduction of

relative equivalent weight for all PFSA polymer (EW∗all) and amounts of PFSA polymer in catalyst layer after the tests suggests that main-chain scission occurs.

Hydrogen peroxide vapor (HPV) exposure tests were applied to PFSA polymer membranes. PFSA polymer degradation after the tests was investigated using ion chromatography and total organic carbon analysis for trap water, and using ^{19}F NMR for water/methanol extracts of membranes. Decomposition products other than fluoride ion accounted for a significant portion of degradation weight loss, and their generation rates were not always proportional to fluoride ion release rate (FRR). The differences between the results of FRR and other decomposition product analysis strongly suggest the presence of two or more decomposition mechanisms in PFSA degradation.

5.3. Conclusions of chapter 4

A sulfonated aromatic block copolymer (SABC), consists of hydrophobic and hydrophilic blocks, whose chemical structure was investigated by 2D NMR of heteronuclear single-quantum correlation (HSQC), heteronuclear multiple-bond correlation (HMBC) and HSQC total correlation spectroscopy (HSQC–TOCSY). Because of its complicated chemical structure with five different phenylene rings, 12 types of ^{1}H signals and 24 types of ^{13}C signals were observed in a narrow chemical shift range (7.0–8.0 ppm for ^{1}H and 118–162 ppm for ^{13}C). To improve the ^{1}H signal separation, the temperature conditions for the ^{1}H nuclear magnetic resonance (NMR) experiments were optimized. Moreover, ^{1}H and ^{13}C NMR signal assignments for the hydrophobic blocks were performed using HSQC and HMBC, with reference to the assignments of a model oligomer. For the hydrophilic blocks, furthermore, HSQC–TOCSY techniques were applied. As a result of these studies, complete ^{1}H and ^{13}C NMR signal assignments were made for the SABC. The ion-exchange capacity (IEC) and the copolymerization composition were calculated using the ^{1}H NMR assignments for the SABC, and the IEC value obtained in this way was consistent with that obtained via titration.

5.4. Conclusions of this study

As the above result showed, the chemical structures of pristine PFSA and SABC were determined. Moreover, all of the NMR signals for the pristine PFSA and SABC were assigned, which is indispensable when studying degradation. Given the results, the following two structural analysis techniques by two-dimensional NMR were proposed: the structural analysis of fluorine compounds and hydrocarbon polymers which possess complicated structures.

Moreover, we made it possible to show the side chain fragments of PFSA and the degraded structure of SABC, using the result obtained in this study as basic data. It was concluded that the degradation of PFSA was evaluated correctly by quantifying other decomposition products in addition to fluoride ion.

Based on this study, I am sure that the electrolyte membrane of cheap cost with high durability will developed. The results of this study will lead to realization of extensive utilization of proton exchange membrane fuel cell.

5.5. Acknowledgements

I am deeply thankful to Professor Michio Hori, who advised me during this study. I would like to express my gratitude to Professor Atsuo Sounai, Professor Yasuo Takagi and Professor Masanori Kobayashi. I am thankful to Tomohiro Minamide, Hiroshi Nakayama, Dr. Byungchan Bae, Professor Kenji Miyatake, Professor Masahiro Watanabe, Dr. Gen Katagiri, Dr. Kazuyoshi Sushida, Kazuo Kimura, Ken Kawaguchi, Akira Abe, Yoshitsugu Nakagawa, Yoko Sakiyama, Kenji Tanabe, Kenji Ookubo, and Nobuyuki Sato, who collaborated on this study.